PHILOSOPHICAL TRANSACTIONS OF THE ROYAL SOCIETY B BIOLOGICAL SCIENCES

A Model of Intrinsic and Driven Spindling in Thalamocortical Neurons

J. L. Hindmarsh and R. M. Rose

Phil. Trans. R. Soc. Lond. B 1994 **346**, 165-183
doi: 10.1098/rstb.1994.0139

A model of intrinsic and driven spindling in thalamocortical neurons

J. L. HINDMARSH[1] AND R. M. ROSE[2]

School of Mathematics[1] and Department of Physiology[2], University of Wales College of Cardiff, Cathays Park, Cardiff, CF1 1SS, U.K.

SUMMARY

We add a slow hyperpolarization-activated inward current $I_H = g_H m_H(v - v_H)$ to our previous model of rebound bursting (Hindmarsh & Rose *Phil. Trans. R. Soc. Lond.* B **346**, 129–150 (1994*a*)) to give a four-dimensional physiological model, and a corresponding four-dimensional model of the model. The physiological model generates periodic 'bursts of bursts' or 'spindles' resembling those recorded experimentally in thalamocortical (TC) neurons. The model of the model is simplified to a two-dimensional system having a limit cycle which corresponds to the slow spindle oscillation of the physiological model. Analysis of the stability of this two-dimensional model allows us to divide the parameter space of the slope (γ_{m_H}) and shift (θ_{m_H}) parameters of $m_{H_\infty}(v)$ into regions in which the model generates spindles or continuous bursting. This enables us to determine the parameter values required for spindling in the physiological model and to explain the experimentally observed effects of noradrenaline.

Next we examine whether a cell at a stable equilibrium point can be driven into spindling by applying a sinusoidal input at the resonant frequency. This is done by averaging the equations for the driven model of the model. Analysis of the stability of these averaged equations shows how the regions of the $(\theta_{m_H}, \gamma_{m_H})$ parameter space change when the system is driven by a sinusoidal input. This enables us to choose parameter values for a physiological model of a driven spindle.

We show that if the physiological model is modified to include a voltage-dependent time constant for m_H, spindles, similar to those of TC cells, can be obtained with a small Ca^{2+}-activated K^+ current. Finally our knowledge of the form of the bifurcation diagram and the conditions for resonance leads to a new suggestion for the roles of $GABA_A$ and $GABA_B$ inhibitory postsynaptic potentials when TC cells are driven into spindling by neurons of the nucleus reticularis thalami.

1. INTRODUCTION

In the first of this series of papers (Hindmarsh & Rose 1994*a*) we showed how a cell with an $I_T - I_{KCa(T)}$ system of ionic currents rebounds to give either continuous bursting or a sequence of decaying bursts following the application of hyperpolarizing current step. Similar properties occur in cells of the lateral habenula nucleus (Wilcox *et al.* 1988), the nucleus reticularis (Avanzini *et al.* 1989; Bal & McCormick 1993), and the inferior olivary nucleus (Yarom 1991; Gutnick & Yarom 1989).

We now show how the addition of a slow hyperpolarization-activated inward current, I_H results in an $I_T - I_{KCa(T)} - I_H$ model which can generate periodic 'bursts of bursts' or 'spindles'. Thalamocortical (TC) cells have been shown to have I_H (Pollard & Crunelli 1989; McCormick & Pape 1990*a*), and to be capable of spindle generation (Leresche *et al.* 1991; Soltez *et al.* 1991). Note that these 'intrinsic' spindles only occur in about a third of TC cells in the cat (Soltez *et al.* 1991) and should not be confused with the spindles recorded *in vivo* which appear to be driven by spindle activity in the nucleus reticularis thalami (nRT) (Steriade & Deschenes 1984; Steriade *et al.* 1985, 1987, 1988).

Throughout these papers our interest has not been simply to produce a model that simulates experimental recordings but to discover how the model works. Bifurcation diagrams are an essential feature of such a discussion. For instance use of the bifurcation diagram enables us to see that by a suitable choice of parameter values it is possible to produce rebound bursting and spindling without the addition of $I_{KCa(T)}$ (M. A. Alawar, J. L. Hindmarsh & R. L. Rose, in preparation). However, the mechanism is very delicate and is enhanced by the addition of $I_{KCa(T)}$ to give a more robust model.

From the point of view of understanding the dynamics of the model we will see that spindling can be explained as a cyclical movement around an inverted bifurcation diagram (see figure 1). In an alternative model of spindling Destexhe *et al.* (1993) have discussed a mechanism in which spindle

Phil. Trans. R. Soc. Lond. B (1994) **346,** 165–183
Printed in Great Britain

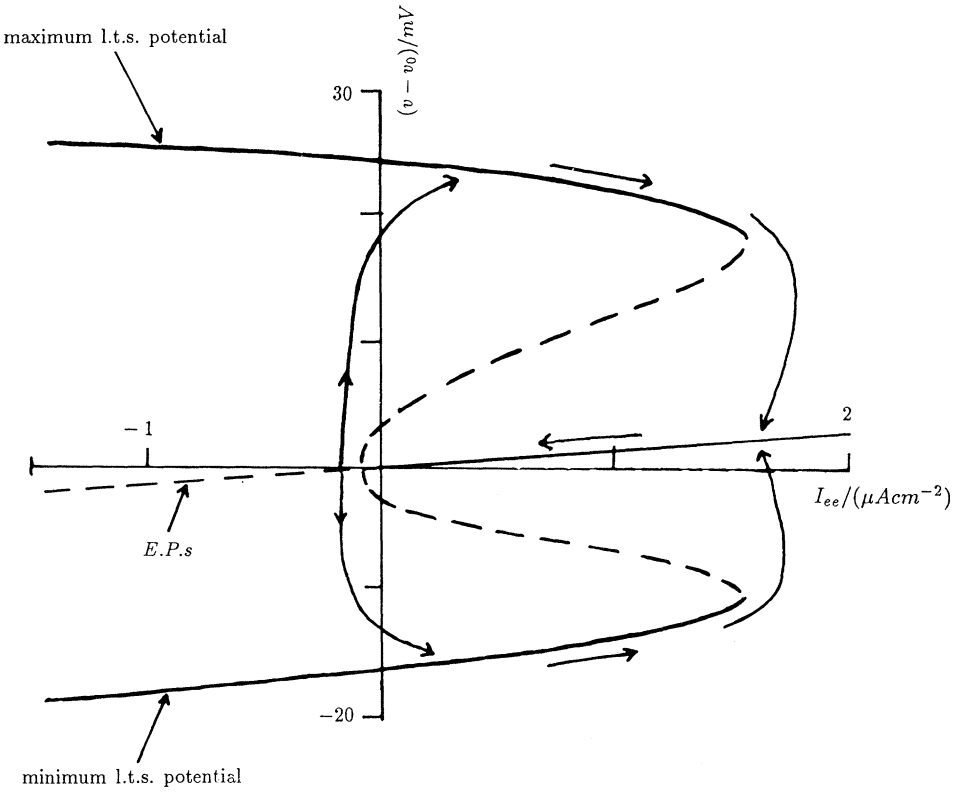

Figure 1. Schematic illustration of the mechansim of spindle generation. The figure shown here is a reproduction of the bifurcation diagram of the three-dimensional model discussed previously (Hindmarsh & Rose 1994*a*) with I replaced by an effective external current I_{ee}. Arrows indicate the possible path of the EP as I_{ee} decreases from $1.6\,\mu A\,cm^{-2}$ to $-0.2\,\mu A\,cm^{-2}$, then they indicate maximum and minimum potentials of the LTSS as I_{ee} increases again.

generation results from a two-variable description of I_H rather than the addition of $I_{KCa(T)}$. In their model spindle generation can also be seen as periodic motion around an inverted bifurcation diagram. However in their model the effect of adding I_H is both to invert a previously non-inverted bifurcation diagram and to provide a mechanism to generate the cyclical movement around this diagram. Our experience is that choosing parameter values so that I_H performs this dual function is a delicate matter (see § 8).

In the model, that we will discuss, spindles are obtained by adding I_H to a model which has a small $I_{KCa(T)}$. In this case the bifurcation diagram, in the (v, I) plane, is already inverted by $I_{KCa(T)}$ before the addition of I_H. The system can be driven around this bifurcation diagram using an m_H variable with either a fixed time constant (as in the simple model of § 5) or using a two variable description of I_H (as in the model of § 8). We think that inverting the bifurcation diagram independently of I_H makes the model more robust. Our final model (figure 7) also appears to bear a closer resemblance to the experimental recordings than the model of Destexhe *et al.* (1993). For instance their model has large-amplitude low threshold spikes (LTSS) and shows marked oscillations during the interspindle period. Neither of these features occur in the real cell (Soltez *et al.* 1991).

The addition of I_H to the $I_T - I_{KCa(T)}$ model results in a four-dimensional system of differential equations. We will see that the intrinsic spindles which this model generates can be thought of as the combination of two limit cycles. That is the oscillation of the LTS is modulated by a much slower oscillation that switches the system alternately between low threshold spiking and silence. Note that addition of further equations for the sodium current would add a very fast oscillation of the action potential. This would give bursts of action potentials on the crest of each low threshold spike. Thus the full model could be thought of as having three distinct limit cycles on three very different timescales. As in the previous papers (Hindmarsh & Rose 1994*a*,*b*) we are mainly interested in the behaviour in the subthreshold region, but in § 8 we will consider a more complete model which has fast action potentials, and compare this model with experimental recordings.

Our main concern is to describe the slowest limit cycle oscillation, which is responsible for the appearance of the spindles. We use the model of the model introduced in Hindmarsh & Rose (1994*a*) to simplify the description of the system. A further simplification is made by taking advantage of the slowness of the activation of I_H. The resulting model is a two-dimensional system of differential equations of polynomial form (see equations (4)). The simplicity of these equations makes it easy to see how they behave, and to calculate parameter values for which they will have the necessary limit cycle. These model

equations also allow us to predict the effect of shifting the activation potential of I_H, and the effect of periodic stimulation of the system.

Besides giving a clearer theoretical understanding of the mechanism of spindling, from an experimental point of view, our knowledge of the form of the bifurcation diagram enables us to predict the conditions under which TC cells will resonate to an applied sinusoidal current. This leads, in the final section, to a new suggestion for the roles of $GABA_A$ and $GABA_B$ inhibitory postsynaptic potentials (IPSPs) when TC cells are driven into spindling by neurons of the nucleus reticularis thalami (Steriade & Deschenes 1984; von Krosigk *et al.* 1993).

2. THE PHYSIOLOGICAL MODEL

Based on the experimental measurements for TC cells of McCormick & Pape (1990*a*) and Soltez *et al.* (1991), we assume that I_H is a mixed Na^+/K^+ current of the form $I_H = g_H m_H(v - v_H)$. As usual g_H is the maximal conductance, m_H the activation variable and v_H the equilibrium potential. Adding this current to equations (4) of Hindmarsh & Rose (1994*a*) gives the following four-dimensional system:

$$\left.\begin{aligned}
\dot{v} &= C^{-1}\{-g_L(v - v_L) - g_K n_\infty^4(v)(v - v_K) \\
&\quad - g_T m_{T_\infty}(v) h_T (v - v_{Ca}) \\
&\quad - g_{KCa(T)}\left(\frac{c}{K_{Ca(T)} + c}\right) \\
&\quad - g_H m_H(v - v_H) + I_0 + I + I(t)\}, \\
\dot{h}_T &= \tau_{h_T}^{-1}(h_{T_\infty}(v) - h_T), \\
\dot{c} &= -k g_T m_{T_\infty}(v) h_T (v - v_{Ca}) - k_{Ca} c, \\
\dot{m}_H &= \tau_{m_H}^{-1}(m_{H_\infty}(v) - m_H),
\end{aligned}\right\} \quad (1)$$

where

$$m_{H_\infty}(v) = \frac{1}{1 + \exp(-\gamma_H(v - \theta_H))}.$$

The parameter values are the same as those of our standard three-dimensional (v, h_T, c) model (Hindmarsh & Rose 1994*a*), except for the new parameters g_H, v_H, τ_{m_H}, γ_H and θ_H whose values will be given below following our discussion of how the model works. Although we will choose values similar to those found experimentally (see table 1), our choice is largely determined by the equations of our standard model. Note that in equations (1) we have used a voltage-independent time constant τ_H^{-1}. We have done this because at this stage our aim is to obtain a simple model that clearly displays what we regard as the underlying mechanism for spindle generation. In §8 we will refine this model to include a voltage-dependent time constant for I_H.

As in Hindmarsh & Rose (1994*a*) we put $I_0 = -1.35\,\mu A\,cm^{-2}$. The equation for $\dot{v}$ then becomes:

$$\begin{aligned}
\dot{v} = C^{-1}\{&-g_L(v - v_L) - g_K n_\infty^4(v)(v - v_K) \\
&- g_T m_{T_\infty}(v) h_T (v - v_{Ca}) \\
&- g_{KCa(T)}\left(\frac{c}{K_{Ca(T)} + c}\right)(v - v_K) + I_0\} \\
&+ C^{-1}(I - g_H m_H(v - v_H)).
\end{aligned}$$

where the terms in brackets { } are the same as in Hindmarsh & Rose (1994*a*) and an equivalent external current,

$$(I - g_H m_H(v - v_H)),$$

has been added. Now rewrite this equivalent external current as:

$$(I - g_H m_H(v - v_H)) = (I - g_H m_H(v - v_L) - g_H m_H(v_L - v_H)).$$

Table 1. *Parameter values for the physiological model*

parameter (units)	physiological model of the undriven spindle	McCormick & Pape (1991*a*) ($n = 7$)	Soltez *et al.* (1992) ($n = 3$)
v_H (mV)	−40	−43 ± 9	−33 ± 1.2
τ_H^{-1} (ms^{-1})	0.0005	0.0005–0.4 (voltage dependent)	0.0001–0.5 (voltage dependent)
γ_H (mV^{-1})	−0.4	−0.17	−0.25
θ_H (mV)	−71	−76 ± 3	−73 ± 4
g_H ($mS\,cm^{-2}$)	0.8[a]	5–25 nS per cell (total membrane conductance)	4–6 nS per cell (total membrane conductance)

[a] The value for this parameter is difficult to estimate. McCormick *et al.* (1992) say that the average total membrane area for cat LGNd cells is 38 000 μm^2 whereas Wang *et al.* (1991) in their model of a thalamic neuron assume a (somatic) membrane area of approximately 1000–2000 μm^2. Using the middle value (1500 μm^2) of this latter area our value for g_H corresponds to 12 nS per cell.

PHILOSOPHICAL TRANSACTIONS OF THE ROYAL SOCIETY B BIOLOGICAL SCIENCES

Then equations (1) become:

$$\left.\begin{aligned}
\dot{v} &= C^{-1}\{-(g_{\mathrm{L}}+g_{\mathrm{H}}m_{\mathrm{H}})(v-v_{\mathrm{L}}) \\
&\quad - g_{\mathrm{K}}n_{\infty}^{4}(v)(v-v_{\mathrm{K}}) \\
&\quad - g_{\mathrm{T}}m_{\mathrm{T}_{\infty}}(v)h_{\mathrm{T}}(v-v_{\mathrm{Ca}}) \\
&\quad - g_{\mathrm{KCa(T)}}\left(\frac{c}{K_{\mathrm{Ca(T)}}+c}\right)(v-v_{\mathrm{K}}) \\
&\quad + I_0 + I - g_{\mathrm{H}}m_{\mathrm{H}}(v_{\mathrm{L}}-v_{\mathrm{H}})\}, \\
\dot{h}_{\mathrm{T}} &= \tau_{h_{\mathrm{T}}}^{-1}(h_{\mathrm{T}_{\infty}}(v)-h_{\mathrm{T}}), \\
\dot{c} &= -kg_{\mathrm{T}}m_{\mathrm{T}_{\infty}}(v)h_{\mathrm{T}}(v-c_{\mathrm{Ca}}) - k_{\mathrm{Ca}}c, \\
\dot{m}_{\mathrm{H}} &= \tau_{m_{\mathrm{H}}}^{-1}(m_{\mathrm{H}_{\infty}}(v)-m_{\mathrm{H}}).
\end{aligned}\right\} \qquad (2)$$

Except for the fact that g_{L} has been replaced by $(g_{\mathrm{L}}+g_{\mathrm{H}}m_{\mathrm{H}})$, we can think of the first three equations (2) as those of equations (4) of Hindmarsh & Rose (1994*a*) driven by an equivalent external current,

$$I_{\mathrm{ee}} = (I - g_{\mathrm{H}}m_{\mathrm{H}}(v_{\mathrm{L}}-v_{\mathrm{H}})).$$

3. A MODEL OF THE MODEL

We want to approximate equations (2) using the model of the model introduced in Hindmarsh & Rose (1994*a*). To justify this we could decrease the value of g_{L} to partially compensate for the $g_{\mathrm{H}}m_{\mathrm{H}}$ term. This of course could not be done exactly because m_{H} is a variable. However we made no alteration to the value of g_{L} and found that everything worked satisfactorily. For the above equivalent external current these equations are:

$$\left.\begin{aligned}
\dot{r} &= -\alpha r(1+ar^2 \\
&\quad - b(z+(I-g_{\mathrm{H}}m_{\mathrm{H}}(v_{\mathrm{L}}-v_{\mathrm{H}}))T_{31}/\gamma)), \\
\dot{\theta} &= -\beta + er^2, \\
\dot{z} &= -\gamma(z-cr^2+dr^4).
\end{aligned}\right\} \qquad (3)$$

The essential idea in the model for spindle generation is as follows. When the system is undergoing low threshold oscillations, the slow variable m_{H} (equations (2)) will gradually increase. The resulting increase in the equivalent external current will drive the oscillations to the right of the $(v=v_0, I_{\mathrm{ee}})$ bifurcation diagram (reproduced from Hindmarsh & Rose (1994*a*) in figure 1). When the equivalent external current reaches a value of approximately $1.6\,\mu\mathrm{A\,cm^{-2}}$ the system will return to a (non-oscillatory) EP. Then the equivalent external current should decrease to approximately $-0.2\,\mu\mathrm{A\,cm^{-2}}$ as the system crosses the left-hand bifurcation point, whereupon the oscillations will restart.

In our model m_{H} will vary (within $[0,1]$) and, as it does so, we want:

$$(I - g_{\mathrm{H}}m_{\mathrm{H}}(v_{\mathrm{L}}-v_{\mathrm{H}})),$$

to vary between approximately $-0.2\,\mu\mathrm{A\,cm^{-2}}$, where it will switch on the low threshold oscillation, and $1.6\,\mu\mathrm{A\,cm^{-2}}$, where it will switch off.

Consistent with this requirement, but not uniquely determined by it, we choose $g_{\mathrm{H}} = 0.8\,\mathrm{mS\,cm^{-2}}$ and $I = -1.4\,\mu\mathrm{A\,cm^{-2}}$, which means that we will want m_{H} to vary between 0.08 and 0.2 (g_{H} may be smaller or larger depending on the initial choice of I).

The behaviour of m_{H} is determined by the differential equation:

$$\dot{m}_{\mathrm{H}} = \tau_{m_{\mathrm{H}}}^{-1}(m_{\mathrm{H}_{\infty}}(v) - m_{\mathrm{H}}).$$

Since $\tau_{m_{\mathrm{H}}}^{-1}$ is small, m_{H} changes slowly by comparison with v. Therefore m_{H} will change towards the average value of $m_{\mathrm{H}_{\infty}}(v)$. This average value depends mainly on whether or not the system is undergoing low threshold oscillations. Having changed variables from (v, h_{T}, c) in equations (2) to (r, θ, z) in equations (3), we need to express v in terms of these variables.

Using transformations (8), (9) and (14) of Hindmarsh & Rose (1994*a*) the membrane potential is given by:

$$v = v_0 + T_{11}^{-1}r\cos\theta + T_{11}^{-1}x(I_{\mathrm{ee}}) + T_{13}^{-1}(z+z(I_{\mathrm{ee}})),$$

but we find that it is sufficient to take:

$$v \approx v_0 + T_{11}^{-1}r\cos\theta,$$

as it is the term $r\cos\theta$ that varies most between oscillatory and non-oscillatory solutions.

The equation for $\dot{m}_{\mathrm{H}}$ can now be written as:

$$\dot{m}_{\mathrm{H}} = \tau_{m_{\mathrm{H}}}^{-1}(m_{\mathrm{H}_{\infty}}(v_0 + T_{11}^{-1}r\cos\theta) - m_{\mathrm{H}}).$$

The steady state value of m_{H} can now be expanded as a Taylor series:

$$m_{\mathrm{H}_{\infty}}(v_0 + T_{11}^{-1}r\cos\theta) \approx m_{\mathrm{H}_{\infty}}(v_0) + T_{11}^{-1}r\cos\theta m'_{\mathrm{H}_{\infty}}(v_0) + \frac{(T_{11}^{-1}r\cos\theta)^2}{2!}m''_{\mathrm{H}_{\infty}}(v_0) + \ldots.$$

Because $\tau_{m_{\mathrm{H}}}^{-1}$ is small, m_{H} changes slowly in time compared with θ. We therefore replace $r\cos\theta$ with its averaged value zero, and $r^2\cos^2\theta$ with its averaged value $r^2/2$. Ignoring higher order contributions from the Taylor series gives the following equation for $\dot{m}_{\mathrm{H}}$:

$$\dot{m}_{\mathrm{H}} = \tau_{m_{\mathrm{H}}}^{-1}(m_{\mathrm{H}_{\infty}}(v_0) + \frac{(T_{11}^{-1})^2}{4}r^2m''_{\mathrm{H}_{\infty}}(v_0) - m_{\mathrm{H}}).$$

Again, using the fact that $\tau_{m_{\mathrm{H}}}^{-1}$ is small we will assume that we can simplify further by putting $z = cr^2 - dr^4$ in equations (3). This means that the behaviour of the system is now described by the two-dimensional system:

$$\begin{aligned}
\dot{r} &= -\alpha r(1+(a-bc)r^2 + bdr^4 \\
&\quad - b(I - g_{\mathrm{H}}m_{\mathrm{H}}(v_{\mathrm{L}}-v_{\mathrm{H}}))T_{31}/\gamma), \\
\dot{m}_{\mathrm{H}} &= \tau_{m_{\mathrm{H}}}^{-1}(m_{\mathrm{H}_{\infty}}(v_0) + \frac{(T_{11}^{-1})^2}{4}r^2m''_{\mathrm{H}_{\infty}}(v_0) - m_{\mathrm{H}}).
\end{aligned}$$

Using the new variable

$$w = m_{\mathrm{H}} - m_{\mathrm{H}_{\infty}}(v_0),$$

PHILOSOPHICAL TRANSACTIONS OF THE ROYAL SOCIETY B BIOLOGICAL SCIENCES

these equations become:

$$\left.\begin{aligned}\dot{r} &= -\alpha r(1+e+(a-bc)r^2+bdr^4+fw),\\ \dot{w} &= \tau_{m_H}^{-1}(hr^2-w),\end{aligned}\right\} \qquad (4)$$

where

$$e = -b(I - g_H m_{H_\infty}(v_0)(v_L - v_H))T_{31}/\gamma,$$

$$f = bg_H(v_L - v_H)T_{31}/\gamma,$$

$$h = \frac{(T_{11}^{-1})^2}{4} m''_{H_\infty}(v_0).$$

4. LIMIT CYCLE OF THE MODEL OF THE MODEL

Equations (4) have EPs at those points whose coordinates satisfy the equations:

$$r(1+e+(a-bc)r^2+bdr^4+fw)=0,$$

and

$$hr^2 - w = 0.$$

There is therefore one EP at $(0,0)$ and, provided that $(1+e)<0$, another at (w_0, r_0), where:

$$1+e+(a-bc+fh)r_0^2+bdr_0^4=0, \qquad (5)$$

and

$$hr_0^2 - w_0 = 0.$$

The reason for this is that:

$$r_0 = \left\{\frac{-(a-bc+fh)+\sqrt{[(a-bc+fh)^2-4bd(1+e)]}}{2bd}\right\}^{1/2}, \qquad (6)$$

is real provided that $4bd(1+e)<0$ or, equivalently $1+e<0$ (as $4bd>0$).

Consideration of the state diagram, in particular the configuration of the nullclines (figure 2*d*) suggests that if it is an unstable node or spiral it will be enclosed by a stable limit cycle. We therefore analyse the stability of this EP.

The linear approximation matrix at (w_0, r_0) is:

$$\boldsymbol{A}(w_0, r_0) = \begin{pmatrix} -\alpha(1+e+3(a-bc)r_0^2+5bdr_0^4+fw_0 & -\alpha f r_0 \\ 2\tau_{m_H}^{-1} h r_0 & -\tau_{m_H}^{-1}\end{pmatrix}.$$

Using the facts that r_0 and w_0 satisfy equations (5), we find that the determinant of this matrix is:

$$2\alpha\tau_{m_H}^{-1}(bdr_0^4-(1+e)),$$

which is positive for $1+e<0$ (the condition for real r_0). Note also that this means that the EP is not a saddle point. Thus the condition that (w_0, r_0) is an unstable EP is simply that the trace of the matrix $\boldsymbol{A}(w_0, r_0)$ is positive. Again using equations (5), this condition for instability is:

$$2\alpha(a-bc+2bdr_0^2)r_0^2 > \tau_{m_H}^{-1}.$$

For sufficiently small $\tau_{m_H}^{-1}$ this gives:

$$r_0^2 < \frac{-(a-bc)}{2bd}.$$

Substituting equation (6) we obtain:

$$\frac{(a-bc)((a-bc)+2fh)}{4bd} < (1+e).$$

Since the determinant of $\boldsymbol{A}(w_0, r_0)$ is positive for $(1+e)<0$, the conditions for the EP to be unstable are:

$$(a-bc)((a-bc)+2fh) < (1+e) < 0. \qquad (7)$$

In this expression the values of a, b, c, d and f have already been fixed as discussed in § 3. The values of e and h depend on the values of γ_{m_H} and θ_{m_H} which have not so far been specified. Values of γ_{m_H} in $[0, 1]$ and θ_{m_H} in $[-80\,\text{mV}, -60\,\text{mV}]$ for which these inequalities (equation (7)) are satisfied are shown as the shaded region in figure 2*a*. The nullclines of equations (4) are shown in figure 2*d* for the choice of $(\theta_{m_H}, \gamma_{m_H})$ represented by the point $(-74\,\text{mV}, -0.25\,\text{mV}^{-1})$ in the shaded region of figure 2*a*. Also shown in figure 2*d* are some state paths emerging from the region near the r nullcline, and the limit cycle. Note that although the limit cycle lies very close to the w axis it does not touch it. In fact the separatrix from the saddle point wraps infinitely around the outside of the limit cycle.

The $(\theta_{m_H}, \gamma_{m_H})$ diagram of figure 2*a* is divided into regions where $1+e>0$ and where $1+\epsilon<0$ by the solid curve. Immediately to the left of this curve is the shaded region of parameter values giving limit cycles and nullclines such as those shown in figure 2*d*. We will show in the next section that the physiological model generates spindles for parameter values in this region. For points to the left of this region the nullclines intersect at a stable EP with $r>0$, as shown in figure 2*c*. In the physiological model this corresponds to the cell generating continuous low threshold oscillations. Finally in the region where $1+e>0$, the nullcline configuration is as shown in figure 2*e*, with a single stable EP on the r axis. Here the corresponding physiological model also has a stable EP.

We note that the three nullcline diagrams shown in figure 2*c–e* correspond to the same value of the slope parameter γ_{m_H}, and differ only in the parameter θ_{m_H} which locates the activation curve $m_{H_\infty}(v)$.

5. THE PHYSIOLOGICAL MODEL OF THE UNDRIVEN SPINDLE

The parameter values a, b, c and d in the model of the model of Hindmarsh & Rose (1994*a*) apply at $v_0 = -63.3\,\text{mV}$, $v_L = -59\,\text{mV}$, $I_0 = -1.35\,\mu\text{A cm}^{-2}$ and $I = 0\,\mu\text{A cm}^{-2}$.

In the model of § 3 (equations (3)) of this paper we used a value of $I = -1.4\,\mu\text{A cm}^{-2}$, which amounts to a constant external current $(I + I_0)$ of $-2.75\,\mu\text{A cm}^{-2}$. A physiological model with external current of $0\,\mu\text{A cm}^{-2}$ is obtained by adjusting the value of v_L

PHILOSOPHICAL TRANSACTIONS OF THE ROYAL SOCIETY B BIOLOGICAL SCIENCES

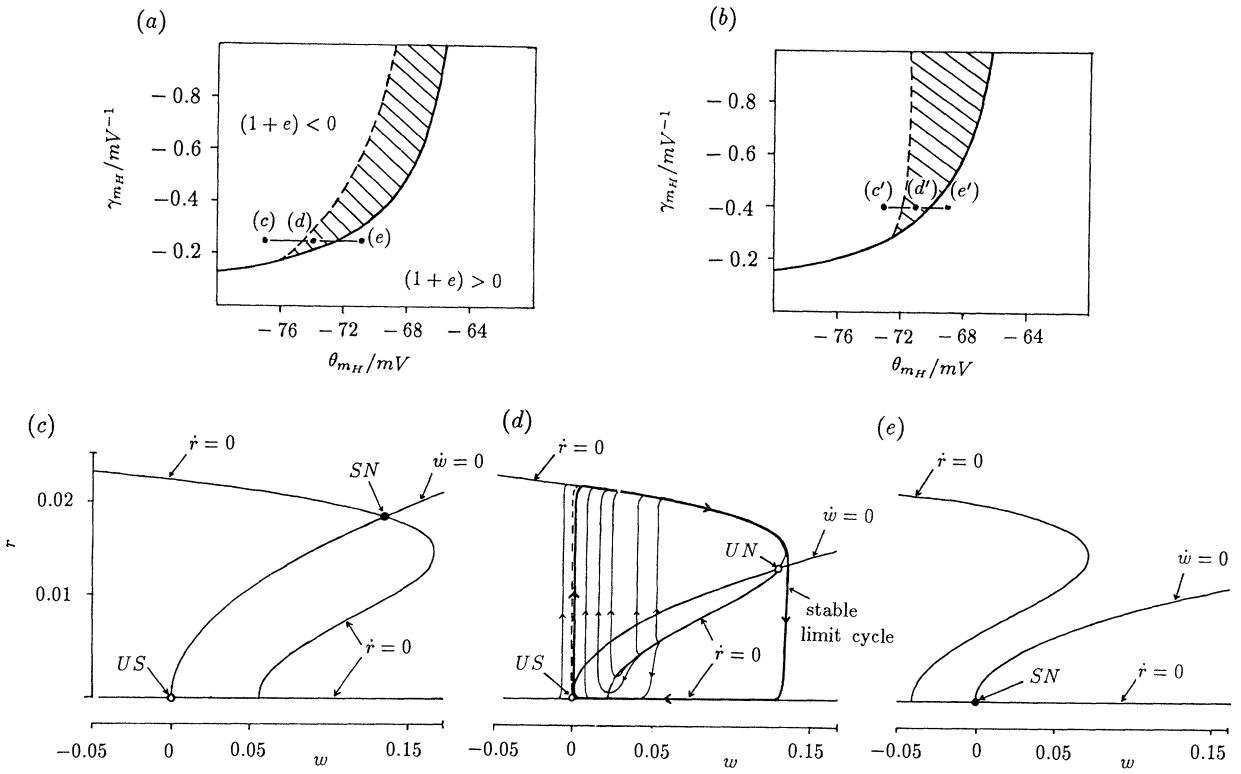

Figure 2. Models for the undriven spindle. (*a*) $(\theta_{m_H}, \gamma_{m_H})$ parameter space for the model of the model showing the region, obtained analytically, where the single EP of equations (4) is unstable (hatched region). (*b*) $(\theta_{m_H}, \gamma_{m_H})$ parameter space for the physiological model showing the region where numerical integration of equations (1) exhibits spindles (hatched region). (*c*) Nullcline diagram for the point labelled (*c*) in (*a*) $(\theta_{m_H} = -77\,\text{mV}, \gamma_{m_H} = -0.25\,\text{mV}^{-1})$. Nullclines intersect at a stable node or spiral (SN) and an unstable saddle point (US). (*d*) Nullcline diagram for the point labelled (*d*) in (*a*) $(\theta_{m_H} = -74\,\text{mV}, \gamma_{m_H} = -0.25\,\text{mV}^{-1})$. Nullclines intersect at an unstable node or spiral (UN) and an unstable saddle point (US). Numerical integration of equations (4) show that the UN is surrounded by a stable limit cycle. Separatrix leaving the US point indicated by the vertical dashed line. (*e*) Nullcline diagram for the point labelled (*e*) in (*a*) $(\theta_{m_H} = -71\,\text{mV}, \gamma_{m_H} = -0.25\,\text{mV}^{-1})$. Nullclines intersect at a single SN on the w axis. Parameter values are given in table 1 and the Appendices of Hindmarsh & Rose (1994*a*) except that $I = -1.4\,\mu\text{A cm}^{-2}$ and $v_L = -59\,\text{mV}$ for the model of the model and $I = 0\,\mu\text{A cm}^{-2}$ and $v_L = -70\,\text{mV}$ for the physiological model.

from −59 mV to v'_L given by:

$$-g_L(v_0 - v_L) - 2.75 = -g_L(v_0 - v'_L).$$

Thus $v'_L = -70\,\text{mV}$.

We replace v_L in equations (1) with this new value and set the external current to zero. Using the same parameter value for g_H, figure 2*b* shows the regions in the $(\theta_{m_H}, \gamma_{m_H})$ parameter space for which the physiological model is continuously bursting (top left-hand region), generates spindles (hatched region) or is silent (to the right of the solid curve). This figure was obtained by numerical integration of equations (1) by exploring parameter values for $(\theta_{m_H}, \gamma_{m_H})$ suggested by the results from the model of the model shown in figure 2*a*. In view of the approximations made it is not surprising that figures 2*a* and 2*b* are not identical. However they do exhibit a similar configuration of the various regions.

For the point (*d′*) in figure 2*b*, where $(\theta_{m_H}, \gamma_{m_H}) = (-0.4\,\text{mV}^{-1}, -71\,\text{mV})$, numerical integration of equations (1) gives the spindle oscillation for the physiological model (figure 3*b*). This oscillation is similar to the spindles recorded experimentally in TC cells (Soltez *et al.* 1991, figure 8). In particular the envelop of LTS amplitudes is similar, and the downward drift of the membrane potential between v_1 and v_3 is a characteristic feature of the recorded spindles.

To explain these features we first draw the (v, m_H) bifurcation diagram (figure 3*a*). This diagram is obtained by taking the first three of equations (1) and treating m_H as a bifurcation parameter, rather than a variable, whilst keeping I constant. Then, on the same diagram we show the points whose coordinates are the values of v and m_H between spindles and also the maximum and minimum potentials of the LTSs during spindles.

Starting at time t_1 (figure 3*b*) where the membrane potential is v_1, these points follow the line of EPs of the bifurcation diagram, giving a downward drift of the membrane potential to v_3. They cross the bifurcation point at time t_2, then, after a noticeable delay, separate from what is now an unstable EP of the bifurcation diagram at time t_3. At time t_4 these points are at the upper and lower branches of the stable limit cycles of the bifurcation diagram. Between times t_4 and t_5 they follow these branches before returning to the start at time t_6.

Experimentally Soltez *et al.* (1991) have found that

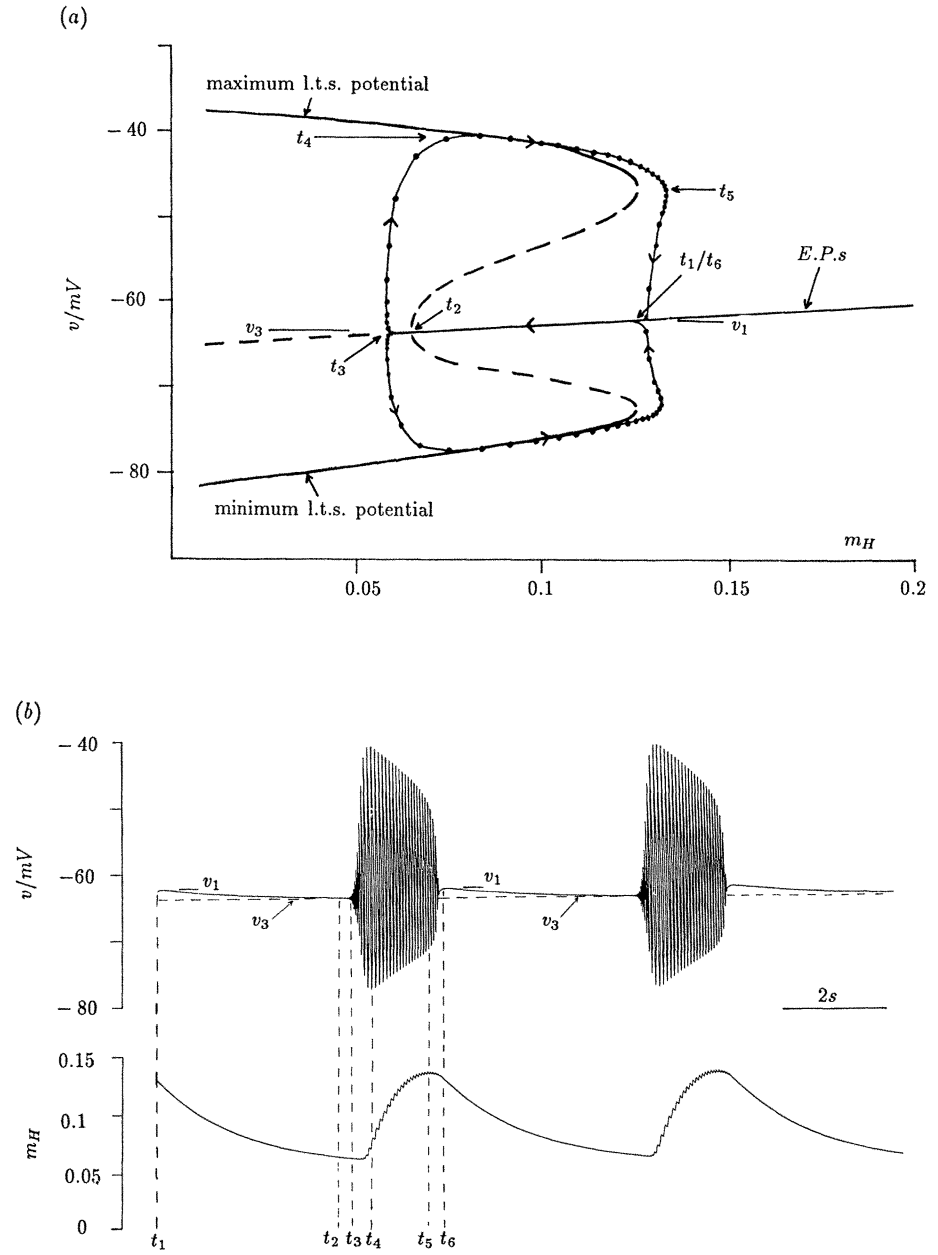

Figure 3. Physiological model of the undriven spindle. (*a*) Changes in membrane potential v and activation m_H during one cycle of the spindle oscillation shown in (*b*). These changes are superimposed on the (m_H, v) bifurcation diagram. For the bifurcation diagram the solid line indicates stable EP or limit cycle and the dashed line indicates unstable EP or limit cycle. For the changes in membrane potential v and activation m_H the successive maxima and minima for the LTSs are shown as solid lines. (*b*) Timecourses of membrane potential v (upper trace) and activation m_H (lower trace) obtained by numerical integration of equations (1). Parameter values are as in figure 2 and for the point (d') in figure 2*b* where $(\theta_{m_H} = -71\,\text{mV}, \gamma_{m_H} = -0.4\,\text{mV}^{-1})$.

noradrenaline has the effect of transforming low threshold oscillations into spindle oscillations and then into a silent state. This happens over a slow time scale (approximately 20 min) and is accompanied by depolarization of the cell and an increase in the amplitude of I_H as measured under voltage clamp conditions. During washout of the neurotransmitter the sequence is reversed.

We can interpret these observations using figure 2 and the fact that noradrenaline has been shown to cause a positive shift of 3–5 mV in $m_{H_\infty}(v)$ (McCormick & Pape 1990*b*). To do this we selected point, (c'), (d'), and (e') in figure 2*b*, along a line of constant slope $(\gamma_{m_H} = -0.4\,\text{mV}^{-1})$ at $\theta_{m_H} = -73$ mV, $\theta_{m_H} = -71$ mV and $\theta_{m_H} = -69$ mV. If the cell was initially at $\theta_{m_H} = -73$ mV it would be continuously oscillating. At $\theta_{m_H} = -71$ mV it would produce spindle oscillations, and at $\theta_{m_H} = -69$ mV it would be silent. Thus we interpret the effects of noradrenaline on TC cells as observed by Soltez *et al.* (1991) as a horizontal movement of θ_{m_H} of 3–5 mV in the $(\theta_{m_H}, \gamma_{m_H})$ diagram as shown in figure 2*b*.

For an interpretation of these results, using the model of the model, we take the points (*c*), (*d*) and (*e*) in figure 2*a* along a line of constant slope $(\gamma_{m_H} = -0.25)$ at $\theta_{m_H} = -77$ mV, $\theta_{m_H} = -74$ mV

and $\theta_{m_H} = -71$ mV. These points correspond to the two-dimensional systems (equations (4)) whose nullcline diagrams are as shown in figure 2*c–e*. Note that as θ_{m_H} increases from -77 mV to -71 mV the w nullcline becomes less steep and the r nullcline moves to the left. This causes the system to change from having a stable EP off the w axis (continuous bursting), through having a stable limit cycle (spindling) to having a stable EP on the w axis (resting).

6. MODEL OF THE MODEL OF A DRIVEN SPINDLE

We now add a periodically varying external current, $\bar{I}\cos\omega t$, to the model described by equations (2) to give:

$$\left.\begin{aligned}
\dot{v} &= C^{-1}\{-(g_L + g_H m_H)(v - v_L) \\
&\quad - g_K n_\infty^4(v)(v - v_k) \\
&\quad - g_T m_{T_\infty}(v) h_T (v - v_{Ca}) \\
&\quad - g_{KCa(T)}\left(\frac{c}{K_{Ca(T)} + c}\right)(v - v_K) \\
&\quad + I_0 + I + \bar{I}\cos\omega t - g_H m_H (v_L - v_H)\}, \\
\dot{h}_T &= \tau_{h_T}^{-1}(h_{T_\infty}(v) - h_T), \\
\dot{c} &= -k g_T m_{T_\infty}(v) h_T (v - v_{Ca}) - k_{Ca} c, \\
\dot{m}_H &= \tau_{m_H}^{-1}(m_{H_\infty}(v) - m_H),
\end{aligned}\right\} \quad (8)$$

The first three of equations (8) are the same as equations (3) of Hindmarsh & Rose (1994*b*) except that g_L has been replaced by $(g_L + g_H m_H)$ and I has been replaced by:

$$I_{ee} = I - g_H m_H (v_L - v_H).$$

In Hindmarsh & Rose (1994*b*) we approximated these three equations by a model of the model in (r, θ, z) coordinates and then averaged the equations. Applying the same approximation, assuming that $g_L \approx (g_L + g_H m_H)$ and using the new variable $w = m_H - m_{H_\infty}(v_0)$, as in § 3 of this paper, we obtain after averaging:

$$\dot{r} = -\alpha r(1 + e + ar^2 - bz + fw) + \frac{\bar{g}}{2}\cos\psi,$$

$$\dot{\psi} = \delta + er^2 + \frac{\bar{g}}{2}\sin\psi,$$

$$\dot{z} = -\gamma(z - cr^2 + dr^4),$$

$$\dot{w} = \tau_{m_H}^{-1}(hr^2 - w).$$

We will not consider a range of driving frequencies but only a frequency near resonance that allows the term $(\bar{g}/2)\cos\psi$ its greatest effect. This happens if ψ is kept small, which is the case when $\delta + er^2 \approx 0$. This of course cannot be achieved for a range of values of r, but by choosing δ so that $\delta + er^2 = 0$ for $r \approx r_{ulc}$ for example we keep ψ near 0.

As before we assume that $z \approx cr^2 - dr^4$ and replace it as such in the equation for $\dot{r}$ leaving us with:

$$\left.\begin{aligned}
\dot{r} &= -\alpha r(1 + e + (a - bc)r^2 - bdr^4 + fw) + \bar{g}/2, \\
\dot{w} &= \tau_{m_H}^{-1}(hr^2 - w).
\end{aligned}\right\} \quad (9)$$

Note that these equations for the driven spindle differ from those for the undriven spindle (equations (4)) by addition of $\bar{g}/2$ to the $\dot{r}$ equation.

We want to start the system at a stable EP when $\bar{g} = 0$. This will be the case if $(1 + e) > 0$, giving a nullcline configuration such as that shown in figure 2*e*.

For $\bar{g} > 0$ there may be either one or three EPs. Suppose that one of these EPs is at (w_0, r_0). At this EP:

$$-\alpha r_0(1 + e + (a - bc)r_0^2 + bdr_0^4 + fw) + \bar{g}/2 = 0,$$

$$w_0 = hr_0^2. \quad (10)$$

Therefore at this EP $\bar{g} = f(r_0)$ where:

$$f(r) = 2\alpha r(1 + e + (a - bc + fh)r^2 + bdr^4). \quad (11)$$

The linear approximation matrix, $\boldsymbol{A}(w_0, r_0)$ for equations (9) is the same as that of equations (4) (§ 3). The EP will be unstable if the trace of $\boldsymbol{A}(w_0, r_0)$ is positive. Since $\tau_{m_H}^{-1} \approx 0$ this gives:

$$(1 + e) + (3(a - bc) + fh)r_0^2 + 5bdr_0^4 < 0. \quad (12)$$

Since $(1 + e) > 0$, the above inequality is satisfied between two (positive) values of r_0 given by:

$$r_\pm^2 = \frac{-[3(a - bc) + fh] \pm \sqrt{[(3(a - bc) + fh)^2 - 20bd(1 + e)]}}{10bd}.$$

We now want to determine the conditions for which equation (12) has real roots, r_- and r_+, and all EPs fall within $[r_-, r_+]$. In the simplest case (C1), in which $f'(r) = 0$ has no real roots, there will be just one unstable EP in $[r_-, r_+]$. If $f'(r) = 0$ has real roots, we begin by finding out if there is a range of $\bar{g}$ values, $[\bar{g}_-, \bar{g}_+]$, with $\bar{g}_- < \bar{g}_+$, such that if $\bar{g} \in [\bar{g}_-, \bar{g}_+]$ then all EPs lie inside $[r_-, r_+]$.

Let r_1 be the point where $f(r)$ has a maximum, and r_2 the point where $f(r)$ has a minimum value. Let $\bar{g}_-$ and $\bar{g}_+$ be defined by:

$$\bar{g}_- = \begin{cases} \max(f(r_1), f(r_-), & \text{if } r_1 < r_- \\ f(r_-), & \text{if } r_- < r_1, \end{cases}$$

$$\bar{g}_+ = \begin{cases} \min(f(r_+), f(r_2), & \text{if } r_+ < r_2 \\ f(r_+), & \text{if } r_2 < r_+. \end{cases}$$

Then if $\bar{g}_- < \bar{g} < \bar{g}_+$, all roots of equations (11) lie in $[r_-, r_+]$. Assuming $\bar{g}_- < \bar{g} < \bar{g}_+$ so that all EPs are in $[r_-, r_+]$, the question is how many EPs are there? Under the following conditions there will be just one unstable EP:

$$r_1 > r_1, \quad r_- > r_2, \quad \text{(C2)}$$

$$r_1 > r_+, \quad r_2 > r_+, \quad \text{(C3)}$$

$$r_2 > r_+, \quad r_1 > r_-, \quad \text{(C4)}$$

$$r_+ > r_2, \quad r_- > r_1. \quad \text{(C5)}$$

PHILOSOPHICAL TRANSACTIONS OF THE ROYAL SOCIETY B BIOLOGICAL SCIENCES

The case where $r_2 > r_+$ and $r_- > r_1$ is excluded as it would require the contradictory condition that $\bar{g}_+ < \bar{g}_-$. Under the following condition the system has three unstable EPs:

$$r_1 > r_-, \quad r_2 < r_+. \tag{C6}$$

In Figure 4*a* the hatched region gives values of γ_{m_H} in $[0, 1]$ and θ_{m_H} in $[-80\,\mathrm{mV}, -60\,\mathrm{mV}]$ for which equations (9), with $\bar{g} = 0$, have an unstable EP surrounded by a stable limit cycle. This region is the same as that of the undriven spindle model shown in figure 2*a*.

The stippled region to the right of the hatched region gives values of γ_{m_H} and θ_{m_H} for which equations (9), with $\bar{g} > 0$, can have one unstable EP in $[r_-, r_+]$ as given by conditions C1–C5 above. Finally the black region gives values of γ_{m_H} and θ_{m_H} for which equations (9), with $\bar{g} > 0$, has three unstable EPs in $[r_-, r_+]$ as given by condition C6. In both the black and stippled regions $1 + e > 0$ and we expect the system to have a stable EP with $\bar{g} = 0$ as in figure 2*a*. With $\bar{g} > 0$, there is the possibility of a limit cycle surrounding one unstable EP if a point lies in the stippled region and of a limit cycle surrounding three unstable EPs if a point lies in the black region.

In our model of the model of the undriven spindle (§4, see figure 2*d*) the point $(-74\,\mathrm{mV}, -0.25\,\mathrm{mV}^{-1})$ gave a limit cycle oscillation. For our model of the model of a driven spindle we choose a point immediately to the right of this point at $(-74\,\mathrm{mV}, -0.25\,\mathrm{mV}^{-1})$. At this point, labelled (e') in figure 4*b*, the system is at a stable EP with $\bar{g} = 0$ as previously shown in figure 2*e*.

With this choice of values of θ_{m_H} and γ_{m_H}, which determine e and h, we now select a value of $\bar{g}$ in $[\bar{g}_-, \bar{g}_+]$. The resulting r and w nullclines intersect at one unstable EP as shown in figure 4*e*. The effect of the driving current $\bar{g}$ has been to change the configuration of the r nullcline from that shown in figure 2*e* (with $\bar{g} = 0$) to the Z-shape of figure 4*e*. Numerical integration of equations (9) show that the unstable EP is surrounded by a stable limit cycle.

Using the same value of $\bar{g}$ with $(\theta_{m_H}, \gamma_{m_H})$ having values $(-74\,\mathrm{mV}, -0.25\,\mathrm{mV}^{-1})$ and $(-74\,\mathrm{mV}, -0.25\,\mathrm{mV}^{-1})$ we obtain the nullcline diagrams of figure 4*c*,*d*. Comparing figures 2*c* and 4*c* we see that the addition of the driving term, $\bar{g}$, only causes a slight movement in the location of the stable node. This can be related to the experimental observation (McCormick & Feester 1990; Soltez & Crunelli

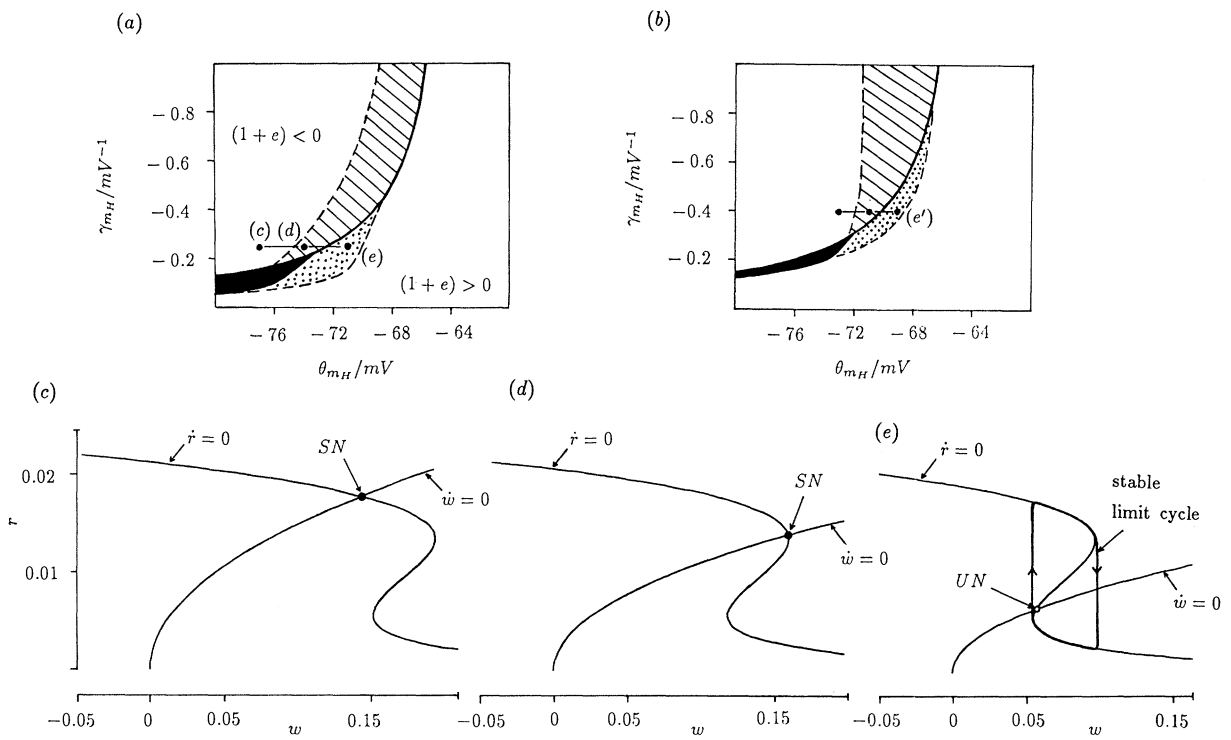

Figure 4. Models of a driven spindle. (*a*) $(\theta_{m_H}, \gamma_{m_H})$ parameter space of the model of the model divided into regions where there is one EP of equations (9) which is unstable when $\bar{g} = 0$ or $\bar{g} = 0.003$ (hatched region), one EP which is stable with $\bar{g} = 0$ but unstable with $\bar{g} = 0.003$ (stippled region) or three unstable EPs with $\bar{g} = 0.003$ (black region). (*b*) $(\theta_{m_H}, \gamma_{m_H})$ parameter space of the physiological model divided into regions where numerical integration of equations (8) gives spindles when $\bar{I} = 0\,\mu\mathrm{A\,cm}^{-2}$ (hatched region), gives a stable resting potential with $\bar{I} = 0\,\mu\mathrm{A\,cm}^{-2}$ but spindling with $\bar{I} = 0.66\,\mu\mathrm{A\,cm}^{-2}$ (stippled region) or a stable resting potential with $\bar{I} = 0\,\mu\mathrm{A\,cm}^{-2}$ but bursting with $\bar{I} = 0.66\,\mu\mathrm{A\,cm}^{-2}$ (black region). (*c*) Nullcline diagram for the point labelled (*c*) in (*a*) $(\theta_{m_H} = -77\,\mathrm{mV}, \gamma_{m_H} = -0.25\,\mathrm{mV}^{-1})$. Nullclines intersect at a stable node or spiral (SN). (*d*) Nullcline diagram for the point labelled (*d*) in (*a*) $(\theta_{m_H} = -74\,\mathrm{mV}, \gamma_{m_H} = -0.25\,\mathrm{mV}^{-1})$. Nullclines intersect at a stable node or spiral (SN). (*e*) Nullcline diagram for the point labelled (*e*) in (*a*) $(\theta_{m_H} = -71\,\mathrm{mV}, \gamma_{m_H} = -0.25\,\mathrm{mV}^{-1})$. Nullclines intersect at an UN surrounded by a stable limit cycle. Parameter values as in figure 2.

1992) that TC cells which are already oscillating remain in the bursting state when receiving synaptic inputs.

Comparing figures 2*d* and 4*d* we see that the effect of the driving current is to switch the system from spindling to continuous bursting. For other parameter choices in this hatched region the effect of the driving term can be simply to shorten the interval between spindles.

Finally note that had we chosen a parameter point in the black region of figure 4*a*, the system would have three unstable EPs. In this case it is possible to have a stable limit cycle surrounding two unstable nodes separated by a saddle point (not shown).

7. THE PHYSIOLOGICAL MODEL OF THE DRIVEN SPINDLE

We now set all parameters, except θ_{m_H} and γ_{m_H}, to the values used in § 5. This includes the adjustment of v_L to -70 mV and I_{Ext} to zero. Guided by the model of the model we chose a driving current in equations (8) of $\bar{I} = 0.66\,\mu A\,cm^{-2}$ and frequency $f = 30$ Hz. Figure 4*b* shows the regions in $(\theta_{m_H}, \gamma_{m_H})$ parameter space for which the physiological model is continuously bursting (top left region), would generate intrinsic spindles with $\bar{I} = 0\,\mu A\,cm^{-2}$ (hatched region), is stable with $\bar{I} = 0\,\mu A\,cm^{-2}$ but is driven into spindling with $\bar{I} = 0.66\,\mu A\,cm^{-2}$ (dotted region), is stable with

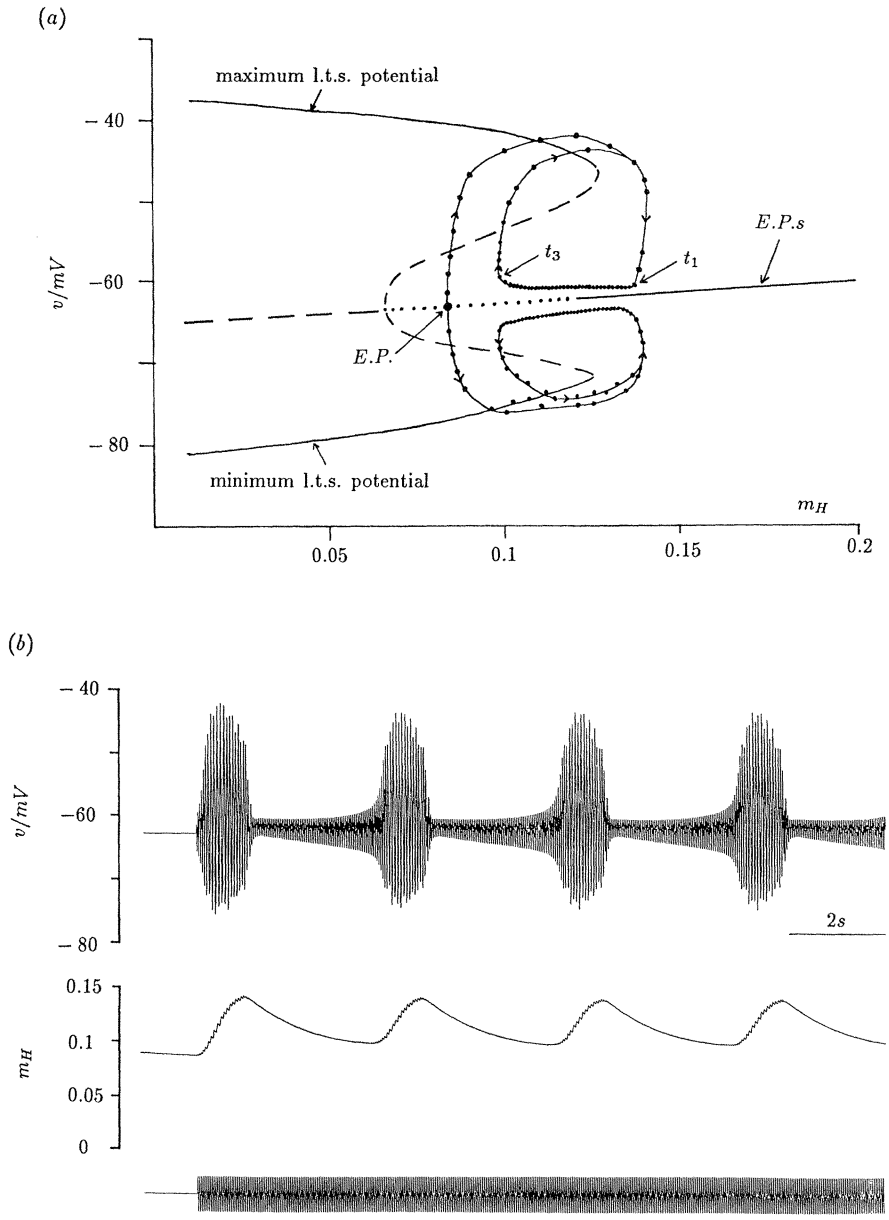

Figure 5. Physiological model of the driven spindle. (*a*) (m_H, v) bifurcation diagram used to illustrate the changes in membrane potential v and activation m_H during one cycle of the driven spindle shown in (*b*). This figure uses the same notation as figure 3*a*. The system is initially at the stable EP indicated before being driven into a limit cycle. (*b*) Timecourses of the membrane potential v (upper trace) and activation m_H (lower trace) obtained by numerical integration of equations (8) for the point labelled (e') in figure 4*b* where $\theta_{m_H} = -69$ mV and $\gamma_{m_H} = -0.4\,mV^{-1}$. The system is driven into spindling by a sinusoidal input of amplitude $\bar{I} = 0.66\,\mu A\,cm^{-2}$ and frequency $f = 30$ Hz as indicated below the figure. Parameter values are as in figures 2 and 3.

PHILOSOPHICAL TRANSACTIONS OF THE ROYAL SOCIETY B BIOLOGICAL SCIENCES

$\bar{I} = 0\,\mu A\,cm^{-2}$ but is driven into continuous bursting with $\bar{I} = 0.66\,\mu A\,cm^{-2}$ (black region) and finally is stable with $\bar{I} = 0\,\mu A\,cm^{-2}$ and gives only a small subthreshold response with $\bar{I} = 0.66\,\mu A\,cm^{-2}$ (bottom right-hand region). This figure was obtained by numerical integration of equations (8) by exploring parameter values for $\theta_{m_H}, \gamma_{m_H}$) suggested by the results from the model of the model shown in figure 4*a*. In view of the approximation made it is not surprising that figures 4*a* and 4*b* are not identical. However they do exhibit a similar configuration of the various regions. It should be noted that for parameter values in the black region the model of the model is driven into spindling whereas the physiological model is driven to bursting.

For example choosing the point (e') in the dotted region of figure 4*b* where $(\theta_{m_H}, \gamma_{m_H}) = (-69\,mV, -0.4\,mV^{-1})$ the system has a stable EP without the driving current and is driven from this stable EP into a spindle oscillation with the driving current (figure 5*b*). Figure 5*a* shows the corresponding (v, m_H) bifurcation diagram. This diagram has been drawn in the same way as figure 3*a*, with which it can be compared. We see that to begin with the system is at a stable EP of the bifurcation diagram, which is well inside the region in which we expect resonance to occur (Hindmarsh & Rose 1994*b*). Application of the sinusoidal input current causes the points at which the membrane potential has a maximum or minimum to move outwards towards the upper and lower branches of the stable limit cycles of the bifurcation diagram. The points then cross these branches and approach the line of stable EPs of the bifurcation diagram.

The most significant difference between the undriven and driven spindle is that these points do not reach this line of stable EPs in the case of the driven spindle. Instead, between times t_1 and t_3 they gradually separate from this line and enter a smaller limit cycle (figure 5*a*) than that of the undriven spindle (figure 3*a*). This difference was predicted by the model of the model as can be seen by comparing the nullcurve configurations of figures 2*e* and 4*e*.

8. AN ALTERNATIVE FOUR-DIMENSIONAL PHYSIOLOGICAL MODEL

Destexhe *et al.* (1993) have recently discussed several alternative models of intrinsic spindling in TC cells. The simplest of these models has three ionic currents I_T, I_H and a slow outward current I_{K_2} (Huguenard & Prince 1991). In this model I_T is described by the four-dimensional model of Wang *et al.* (1991), I_H by a slow and a fast variable and I_{K_2} by three additional variables. This gives a nine-dimensional model.

We now show that it is possible to simplify this model to a four-dimensional system by removing I_{K_2} and using a simpler description for I_T.

In their paper I_H is given by $g_H s f(v - v_H)$ where s and f are slow and fast variables satisfying the differential equations:

$$\dot{s} = \tau_s^{-1}(m_{H_\infty} - s),$$

$$\dot{f} = \tau_f^{-1}(m_{H_\infty} - f).$$

Removing the $\dot{c}$ equation and $I_{KCa(T)}$ from the $\dot{v}$ equation of our physiological model (equations (1)) and replacing our simple description of I_H with that given above we obtain:

$$\left.\begin{aligned}
\dot{v} &= C^{-1}\{-g_L(v - v_L) - g_K n_\infty^4(v)(v - v_K) \\
&\quad - g_T m_{T_\infty}(v) h_T(v - v_{Ca}) \\
&\quad - g_{KCa(T)}\left(\frac{c}{K_{Ca(T)} + c}\right) \\
&\quad - g_H s f(v - v_H) + I_{Ext}\}, \\
\dot{h}_T &= \tau_{h_T}^{-1}(h_{T_\infty}(v) - h_T), \\
\dot{s} &= \tau_s^{-1}(v)(m_{H_\infty} - s), \\
\dot{f} &= \tau_f^{-1}(v)(m_{H_\infty} - f),
\end{aligned}\right\} \qquad (13)$$

where:

$$m_{H_\infty}(v) = \frac{1}{1 + \exp[(v + 69.9)/4]},$$

$$\tau_s^{-1}(v) = \exp[(v + 184.6)/15.24],$$

$$\tau_f^{-1}(v) = \frac{\exp[(v + 159.6)/11.2]}{(1 + \exp[(v + 76)/5.5])},$$

and $g_T = 0.3\,mS\,cm^{-2}$, $g_H = 4\,mS\,cm^{-2}$ and $v_H = -43\,mV$. All other parameter values are given in Appendix 1 of Hindmarsh and Rose (1994*a*). These equations will generate spindles for I_{Ext} between $-4.75\,\mu A\,cm^{-2}$ and $-3.9\,\mu A\,cm^{-2}$, a smaller range than our four-dimensional model. Figure 6*a* shows the result of numerical integration of equations (13) with $I_{Ext} = -4.7\,\mu A\,cm^{-2}$. Also shown are the timecourses of s, f and their product. Note that the timecourse of the product is not unlike the time course of m_H in our four-dimensional model.

We also find that if the system is generating spindles and I_{Ext} is changed to $I_{Ext} = -4.255\,\mu A\,cm^{-2}$ these spindles will terminate and later go into a small amplitude slowly damped oscillation (figure 6*b*). This is almost identical to the behaviour shown in figures 4*a* and 8*a* of Destexhe *et al.* (1993) for their more elaborate models.

In the next section we will investigate the effect of adding an $I_{KCa(T)}$ current to the above four-dimensional model to give a six-dimensional model which, unlike our first model of §2, has the above voltage-dependent time constants $\tau_s(v)$, $\tau_f(v)$ for the activation of I_H.

9. PHYSIOLOGICAL MODEL WITH COMPLEX KINETICS FOR I_H

At the end of our first paper (Hindmarsh & Rose 1994*a*) we discussed a four-dimensional model obtained by adding $I_{KCa(T)}$ to a simplified version of a model given by Wang (1994). We will now show that adding the hyperpolarization-activated cation current I_H, with the complex kinetics described above,

PHILOSOPHICAL TRANSACTIONS OF THE ROYAL SOCIETY B BIOLOGICAL SCIENCES

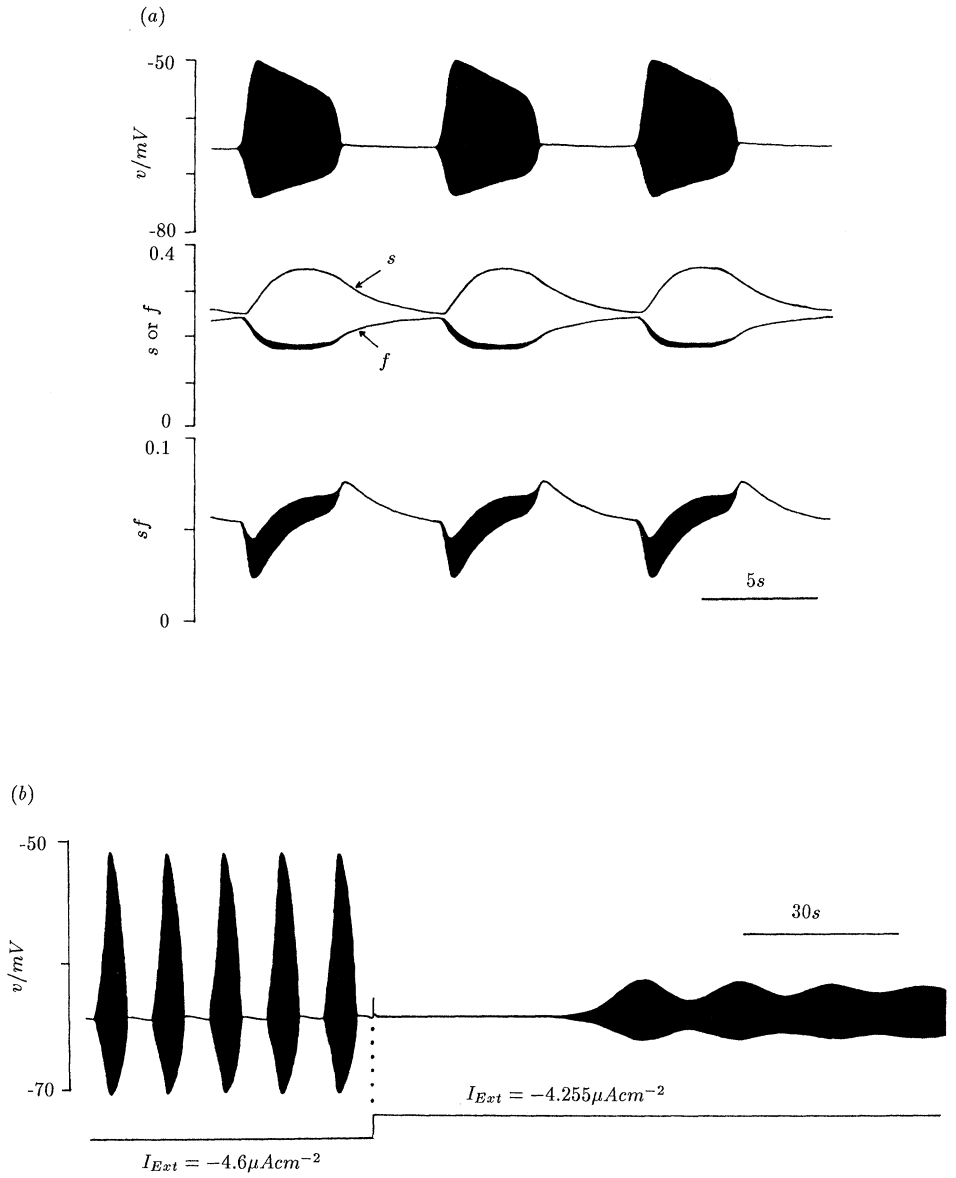

Figure 6. (*a*) Four-dimensional model of the undriven spindle obtained by numerical integration of equations (13). Upper trace shows the timecourse of the membrane potential v. Middle trace shows the timecourses of the slow (s) and fast (f) variables. Lower trace shows the timecourse of the product sf. Parameter values are given in the text. (*b*) See text for explanation.

to this four-dimensional model will produce spindles of low threshold spikes together with action potentials. The equations for this six-dimensional system are:

$$\left.\begin{aligned}
\dot{v} &= C^{-1}\{-I_{\mathrm{Na}} - I_{\mathrm{K}} - I_{\mathrm{L}} - I_{\mathrm{T}} - I_{\mathrm{NaP}} \\
&\quad - I_{\mathrm{KCa(T)}} - I_{\mathrm{H}} + I_{\mathrm{Ext}} + I(t)\}, \\
\dot{n} &= \phi_n \tau_n^{-1}(v)(n_\infty(v) - n), \\
\dot{h}_{\mathrm{T}} &= \phi_{h_{\mathrm{T}}} \tau_{h_{\mathrm{T}}}^{-1}(v)(h_{\mathrm{T}_\infty}(v) - h_{\mathrm{T}}), \\
\dot{c} &= -kI_{\mathrm{T}} - k_{\mathrm{Ca}}c, \\
\dot{s} &= \tau_s^{-1}(v)(m_{\mathrm{H}_\infty} - s), \\
\dot{f} &= \tau_f^{-1}(v)(m_{\mathrm{H}_\infty} - f).
\end{aligned}\right\} \qquad (14)$$

The parameter values for I_{Na}, I_{K}, I_{L}, I_{T}, I_{NaP} and $I_{\mathrm{KCa(T)}}$ are as given in Appendix 3 of Hindmarsh & Rose (1994*a*) except that $g_{\mathrm{Na}} = 50\,\mathrm{mS\,cm^{-2}}$, $g_{\mathrm{NaP}} = 4\,\mathrm{mS\,cm^{-2}}$, $\sigma_{\mathrm{NaP}} = -3\,\mathrm{mV}$, $g_{\mathrm{KCa(T)}} = 0.3\,\mathrm{mS\,cm^{-2}}$, $k_{\mathrm{Ca}} = 0.01\,\mathrm{mS^{-1}}$ and with $v_{\mathrm{sep}} = 0\,\mathrm{mV}$. These adjustments were made to make the threshold for the action potential similar to that of the recording of Soltez *et al.* (1991, figure 8) and to make $I_{\mathrm{KCa(T)}}$ as small as possible.

The definitions of $m_{\mathrm{H}_\infty}(v)$, $\tau_s^{-1}(v)$ and $\tau_f^{-1}(v)$ for the hyperpolarization-activated current I_{H} are:

$$m_{\mathrm{H}_\infty}(v) = \frac{1}{1 + \exp[(v+75)/6.7]},$$

$$\tau_s^{-1}(v) = \exp(v + 189.7)/15.24],$$

$$\tau_f^{-1}(v) = \frac{\exp[(v+164.7)/11.2]}{(1 + \exp[(v+81.1)/5.5])},$$

and $g_{\mathrm{H}} = 0.7\,\mathrm{mS\,cm^{-2}}$ and $v_{\mathrm{H}} = -43\,\mathrm{mV}$. The expressions for $m_{\mathrm{H}_\infty}(v)$, $\tau_s^{-1}(v)$ and $\tau_f^{-1}(v)$ are as given by Destexhe *et al.* (1993) except that they have

been shifted to the left along the voltage axis by 6.1 mV.

Numerical integration of these equations gives the results shown in figure 7. The spindles (upper trace) are similar to the recording shown in figure 8 of Soltez *et al.* (1991). Although the LTSs and the action potentials are similar to the experimental recording, the inter-spindle frequency (0.07 Hz) and the intra-spindle frequency (10 Hz) both have higher values than found experimentally. Note however that Wang (1993) has shown that small adjustments to g_T and g_L can convert the frequency of the low threshold oscillation from 10 Hz to 3 Hz. It may be possible to lower the intra-spindle frequency in this way. Alternatively the addition of I_{K_2} (Huguenard & Prince 1991) may have a similar effect.

10. REVERSE SPINDLING

In this section we present an interesting variation on the above models for spindle generation that is consistent with observations on neurons of the nucleus reticularis thalami (von Krosigk *et al.* 1993). This model uses a similar mechanism to the models above, that is, a slow current driving the system around a bifurcation diagram, but in the reverse direction.

We begin with the two dimensional simplified thalamic model of Hindmarsh & Rose (1994*a*):

$$\left.\begin{aligned}\dot{v} &= C^{-1}\{-g_L(v-v_L) - g_K n_\infty^4(v)(v-v_K) \\ &\quad - g_T m_{T_\infty}(v) h_T (v-v_{Ca}) + I_0 + I + I(t)\}, \\ \dot{h}_T &= \tau_{h_T}^{-1}(h_{T_\infty}(v) - h_T).\end{aligned}\right\} \quad (15)$$

By changing the separation between $m_{T_\infty}(v)$ and $h_{T_\infty}(v)$ we change the bifurcation diagram from that shown in figure 1 of Hindmarsh & Rose (1994*a*) to that shown in figure 8*a*. This bifurcation diagram is indented at both ends (like the Type C bifurcation diagram of Hindmarsh & Rose (1994*a*)) which raises the possibility of a slow current driving the system around the left-hand end (unlike the mechanisms described above which worked with the right-hand end).

Suppose the system starts near an unstable EP just to the right of the left-hand bifurcation point and so goes into low threshold oscillations. To drive the system to the left in the bifurcation diagram we need a hyperpolarizing current that is activated by these oscillations. Such a current is available in the Ca^{2+}-activated K^+ current $I_{KCa(T)}$, provided that we slow down the rate of change of calcium concentration.

Thus we added $I_{KCa(T)} = g_{KCa(T)}(c/(K_{Ca}+c))(v-v_K)$ to equations (15) and plotted the bifurcation diagram using c as a bifurcation parameter and keeping

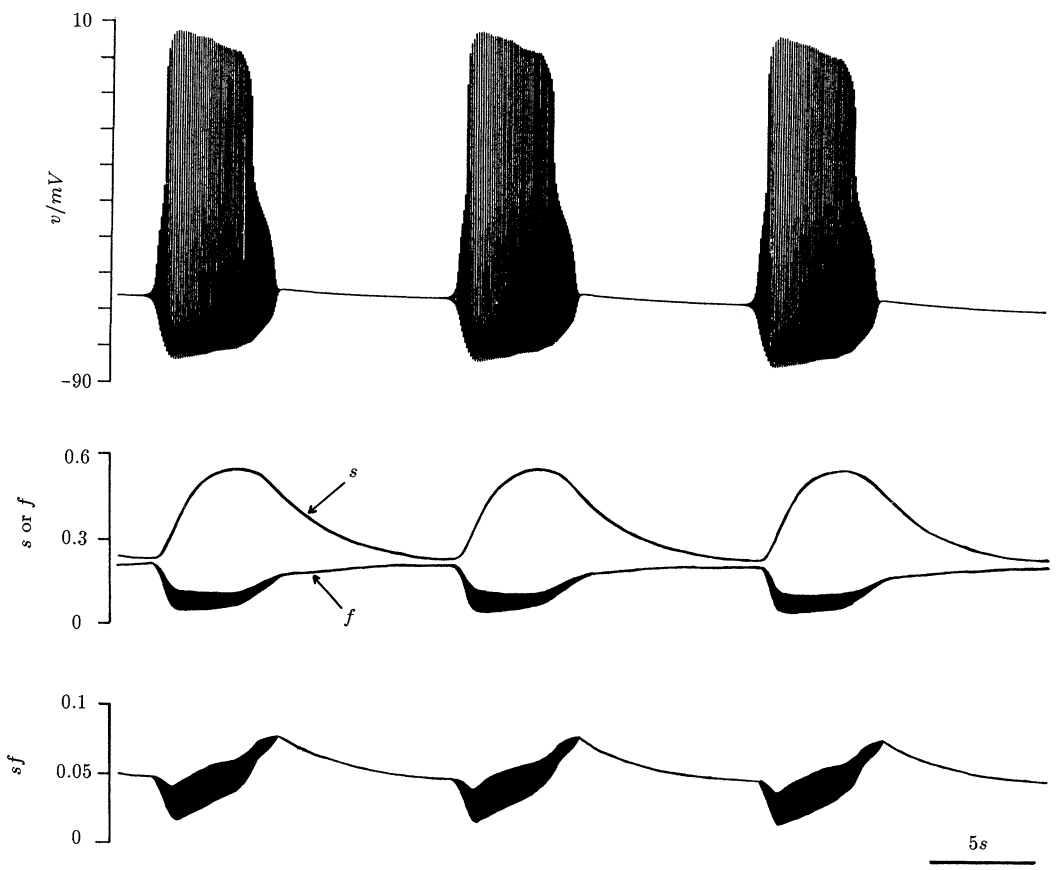

Figure 7. Six-dimensional model of the undriven spindle obtained by numerical integration of equations (14). Upper trace shows the timecourse of the membrane potential v. Middle trace shows the timecourses of the slow (s) and fast (f) variables. Lower trace shows the timecourse of the product sf. Parameter values are given in the text.

PHILOSOPHICAL TRANSACTIONS OF THE ROYAL SOCIETY B BIOLOGICAL SCIENCES

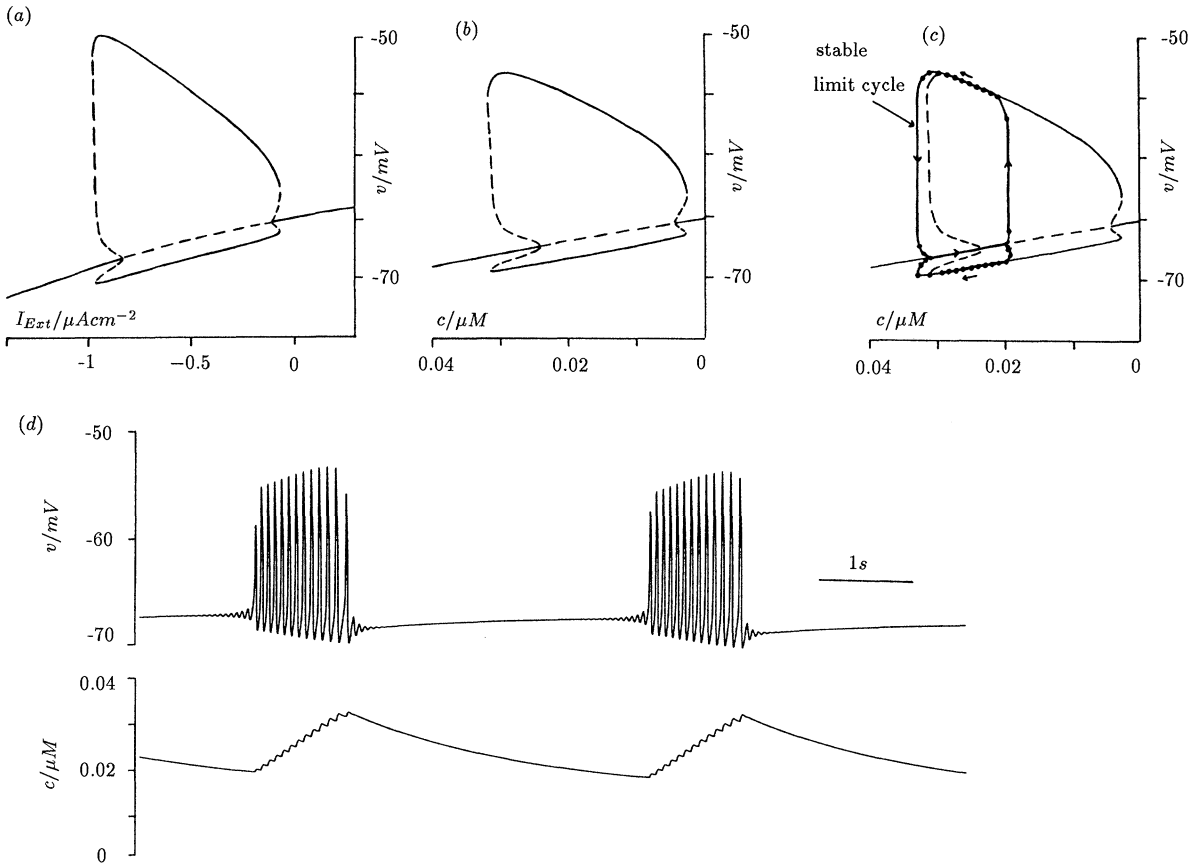

Figure 8. Reverse spindle model. (*a*) $(I_0 + I, v)$ bifurcation diagram for the two-dimensional simplified thalamic model of Hindmarsh & Rose (1994*a*) with $v_{sep} = 1.8\,\mathrm{mV}$ (equations (15) of this paper). Sloping line gives coordinates of EPs whose stability is indicated as: solid line, stable; and dashed line, unstable. The bifurcation diagram is indented at both ends with unstable limit cycles indicated by the dashed curves leaving the line of EPs and stable limit cycles indicated by the outer solid curves. (*b*) (c, v) bifurcation diagram for equations (15) with $I_{\mathrm{KCa(T)}}$ added (see text for explanation). Note that for comparison with (*a*), c increases to the left. (*c*) Changes in the membrane potential, v, and Ca^{2+} concentration, c, during one cycle of the reverse spindle oscillation shown in (*d*). These changes are superimposed on the (c, v) bifurcation diagram shown in (*b*). For the changes in v and c the successive maxima and minima for the LTSs are shown as solid lines. (*d*) Timecourses of membrane potential, v, (upper trace), and Ca^{2+} concentration, c, obtained by numerical integration of equations (16). Parameter values given in text.

the external current fixed (figure 8*b*). This diagram was plotted with c increasing to the left since increasing c corresponds to decreasing $-I_{\mathrm{KCa(T)}}$ (i.e. increasing the hyperpolarizing current $I_{\mathrm{KCa(T)}}$).

Finally adding the equation for $\dot{c}$ we arrive at the system:

$$\left.\begin{aligned}
\dot{v} &= C^{-1}\{-g_{\mathrm{L}}(v - v_{\mathrm{L}}) - g_{\mathrm{K}} n_{\infty}^{4}(v)(v - v_{\mathrm{K}}) \\
&\quad - g_{\mathrm{T}} m_{\mathrm{T}_\infty}(v) h_{\mathrm{T}}(v - v_{\mathrm{Ca}}) \\
&\quad - g_{\mathrm{KCa(T)}}\left(\frac{c}{K_{\mathrm{Ca(T)}} + c}\right)(v - v_{\mathrm{K}}) \\
&\quad + I_0 + I + I(t)\}, \\
\dot{h}_{\mathrm{T}} &= \tau_{h_{\mathrm{T}}}^{-1}(h_{\mathrm{T}_\infty}(v) - h_{\mathrm{T}}), \\
\dot{c} &= -k g_{\mathrm{T}} m_{\mathrm{T}_\infty}(v) h_{\mathrm{T}}(v - v_{\mathrm{Ca}}) - k_{\mathrm{Ca}} c,
\end{aligned}\right\} \qquad (16)$$

where all parameter values are as in Appendix 1 of Hindmarsh & Rose (1994*a*) except that $v_{sep} = 1.8\,\mathrm{mV}$, $k = 0.00001\,\mu\mathrm{M\,cm^{-2}\,\mu A^{-1}\,ms^{-1}}$, $k_{\mathrm{Ca}} = 0.00044\,\mathrm{ms^{-1}}$, $v_{\mathrm{L}} = -67\,\mathrm{mV}$, and $I_{\mathrm{Ext}} = 0\,\mu\mathrm{A\,cm^{-2}}$.

Figure 8*d* shows the timecourse of the resulting spindle together with the timecourse of c. The cyclical movement around the left hand end of the bifurcation diagram is shown in figure 8*c*. Note that this movement is in the reverse direction to that of our earlier models above (compare figure 3*a*).

Recently von Krosigk *et al.* (1993) have shown recordings from neurons of the ferret perigeniculate nucleus which are similar to these reverse spindles. They remark that the progressive hyperpolarization during the spindle oscillation presumably represents the activation of a Ca^{2+}-activated K^+ current by low threshold Ca^{2+} spikes. This is consistent with our model in which $I_{\mathrm{KCa(T)}}$ has this function. Previously Steriade *et al.* (1987) have also suggested that some cells in the intact nRT may generate spindle oscillations autonomously. In our model the same system of equations (equations (16)) may be used to give reverse spindling, which we compare with the recordings from nRT cells by von Krosigk *et al.*

(1993), and, using a different set of parameters, rebound bursting with a tonic tail, which we compared (Hindmarsh & Rose 1994*a*) with the recordings from nRT cells by Bal & McCormick (1993). This suggests that the nRT network, which appears to be the pacemaker for thalamic spindling (Steriade & Deschenes 1984) may be heterogeneous, with some cells being capable of generating intrinsic reverse spindles by the mechanism discussed above, and other cells generating rebound bursting as described in Hindmarsh & Rose (1994*a*).

11. PHYSIOLOGICAL SIGNIFICANCE OF RESONANCE

The problem of how spindling in TC cells is driven by activity in nRT neurons is of importance particularly in relation to absence epilepsy (e.g. Buzsaki *et al.* 1990). So far in this paper we have discussed the resonant response of TC cells to sinusoidal inputs and have not extended the results to synaptic current inputs. Intuitively we would expect resonance to play a significant role when spindles are driven by synaptic inputs under physiological conditions. In this section we briefly outline some of the relevant synaptic physiology of TC cells, and then reinterpret the experimental results in relation to the property of resonance. Although the results are numerical they show how short-duration $GABA_A$ IPSPs could play a prominent role in driven spindling even though the equilibrium potential for these IPSPs is reported to be close to the resting potential of the cell (Crunelli *et al.* 1988).

In vivo investigations in the cat have shown that spindle oscillations in TC cells disappear when these cells are disconnected from the nRT (Steriade *et al.* 1985), and that spindling is preserved in the deafferented nRT (Steriade *et al.* 1987). This has led to the suggestion that GABAergic nRT neurons drive the spindle rhythm in TC cells (Steriade & Deschenes 1984). *In vitro* recordings from the ferret lateral geniculate nucleus (lgn) (von Krosigk *et al.* 1993) have also shown that IPSPs arriving from the perigeniculate nucleus (that part of the nRT associated with the lgn) involve the activation of both $GABA_A$ and $GABA_B$ receptors. These IPSPs could originate from activity in local GABAergic interneurons and/or from GABAergic neurons of the perigeniculate nucleus. However von Krosigk *et al.* (1993) found a lack of activity in presumed interneurons during spindle wave generation.

Detailed information on the properties of $GABA_A$ and $GABA_B$ IPSPs in lgn cells has also been obtained by electrical stimulation of the optic tract (Hirsch & Burnod 1987; Soltez *et al.* 1989). Optic tract stimulation evokes a short-duration IPSP followed by a late longer-lasting IPSP. The short-duration IPSP is Cl^--dependent and involves activation of $GABA_A$ receptors, whereas the long-duration IPSP is K^+-dependent and involves activation of $GABA_B$ receptors (reviewed by Crunelli & Leresche 1991). These IPSPs can be evoked in slices that do not contain the perigeniculate nucleus and, contrary to the findings of von Krosigk *et al.* (1993), are generated by lgn interneurons (Soltez *et al.* 1989).

These experimental results together with the theoretical results discussed so far in this paper led us to consider the following hypothesis. Suppose a cell was at a resting EP which was to the right of the indentation of the bifurcation diagram (see figure 1). Now consider the effects of a periodic train of $GABA_A$ and $GABA_B$ IPSPs. These will have two distinct effects. Firstly the summation of the long-duration $GABA_B$ IPSPs will make the resting potential of the cell more negative and move the EP closer to the bifurcation point. Secondly the short-duration $GABA_A$ IPSPs will act as a periodic stimulus which, if the frequency is suitably chosen, will drive the cell into bursting. This in turn will be terminated by the activation of I_H.

We investigate this hypothesis using our most realistic model of intrinsic spindling (equations (14)). To do so we need to model the $GABA_A$ and $GABA_B$ IPSPs, which we do by adding the current terms I_{GABA_A} and I_{GABA_B} to the equation for $\dot{v}$ in equations (14). The current term I_{GABA_A} is the sum of N currents $I^{(n)}_{GABA_A}$ due to periodic stimuli given at times $t_n = t_0 + nT$ where, in terms of the frequency f, the period $T = 1000/f$ ms and t_0 is a short delay. It is given by:

$$I_{GABA_A} = \sum_{n=1}^{N} I^{(n)}_{GABA_A}, \tag{17}$$

where,

$$I^{(n)}_{GABA_A} = g_{GABA_A} s^{(n)}_A(t)(v - v_{Cl}),$$

$$s^{(n)}_A(t) = \begin{cases} \exp(-(t-t_n)/\tau_{A_1}) - \exp(-(t-t_n)/\tau_{A_2}) & \text{if } t > t_n, \\ 0 & \text{if } t \leqslant t_n, \end{cases}$$

and where g_{GABA_A} is the conductance, $v_{Cl} = -70$ mV, t_n is the arrival time of the stimulus, $\tau_{A_1} = 0.5$ ms and $\tau_{A_2} = 4$ ms.

The current term I_{GABA_B} is similarly given by:

$$I_{GABA_B} = \sum_{n=1}^{N} I^{(n)}_{GABA_B}, \tag{18}$$

where,

$$I^{(n)}_{GABA_B} = g_{GABA_B}(v,f)\, s^{(n)}_B(t)(v - v_K)$$

$$s^{(n)}_B(t) = \begin{cases} \exp(-(t-t_n)/\tau_{B_1}) - \exp(-(t-t_n)/\tau_{B_2}) & \text{if } t > t_n, \\ 0 & \text{if } t \leqslant t_n, \end{cases}$$

and where $g_{GABA_B}(v,f)$ is the conductance which depends on the membrane potential v and the frequency of stimulation f, $v_K = -105$ mV, $\tau_{B_1} = 70$ ms and $\tau_{B_2} = 110$ ms. To explain the nonlinear relationship between the maximum amplitude of the $GABA_B$ IPSP and the cell membrane potential at which the stimulus is applied (Hirsch & Burnod 1987; Soltez *et al.* 1989) we assume that the conductance is given by:

$$g_{GABA_B}(v,f) = \frac{g_{GABA_B}(f)}{1 + \exp(0.035(v+80))}.$$

The $GABA_B$ IPSPs also show a decrease in amplitude with increasing frequency (Hirsch & Burnod 1987; Soltez *et al.* 1989). We assumed that the amplitude was constant for frequencies less than $f_{min} = 5$ Hz and, for all pulses following the first in the train, inversely proportional to the frequency for frequencies above f_{min} giving:

$$g_{GABA_B}(f) = \begin{cases} g_{GABA_B} & \text{for } f \leqslant f_{min}; \\ g_{GABA_B} f_{min}/f & \text{for } f > f_{min}. \end{cases}$$

Equations (14) with I_{GABA_A} and I_{GABA_B} added to the $\dot{v}$ equation were integrated numerically for different values of g_{GABA_A} and f with $I_{Ext} = 1.4\,\mu A\,cm^{-2}$, $g_{GABA_B} = 2.2\,mS\,cm^{-2}$ and $N = 100$. Initially the cell was at rest with membrane potential -60.6 mV. The hatched regions in figure 9*a* are the values of f and g_{GABA_A} for which the cell fired action potentials. Note that the main resonance curve is at approximately 18 Hz with a harmonic at 9 Hz. The region associated with the harmonic is closed showing that if the amplitude is too large the cell will not fire. Figure 9*c* shows an example where $f = 19$ Hz and $g_{GABA_A} = 0\,mS\,cm^{-2}$ (point C in figure 9*a*) and the cell does not fire. The upper trace shows the timecourse of the membrane potential which moves towards the bifurcation point as the slow current I_{GABA_B} summates as shown in the lower trace. Note that I_{GABA_B} is not constant and has a small ripple. This is enough to build up the small oscillation seen in the membrane potential but not enough to fire the cell. Figure 9*b* shows an example where $f = 19$ Hz and $g_{GABA_A} = 0.2\,mS\,cm^{-2}$ (point B in figure 9*a*) and the cell fires. The start of the resulting spindle is shown in the upper trace and the combined synaptic currents I_{GABA_A} and I_{GABA_B} are shown in the lower trace. Note that the magnitude and sign of the g_{GABA_A} synaptic current (the spikes in the lower trace) depend on the value of $(v - v_{Cl})$ when the pulse arrives. Thus even though v_{Cl} is close to the resting potential the magnitude of these pulses can be quite large. The effect of the pulse on the membrane potential depends on the arrival time within the cycle. Pulses arriving on the falling phase build up the oscillation because $(v - v_{Cl})$ is large and positive. For points outside the tuning curve such as points D and E in figure 9*a* this buildup in amplitude does not take place. This is either because the pulses arrive on the rising phase of the oscillation in figure 9*e* (where $f = 16.5$ Hz and $g_{GABA_A} = 0.2\,mS\,cm^{-2}$) or the pulses are of such large amplitude that they reduce the duration of the low

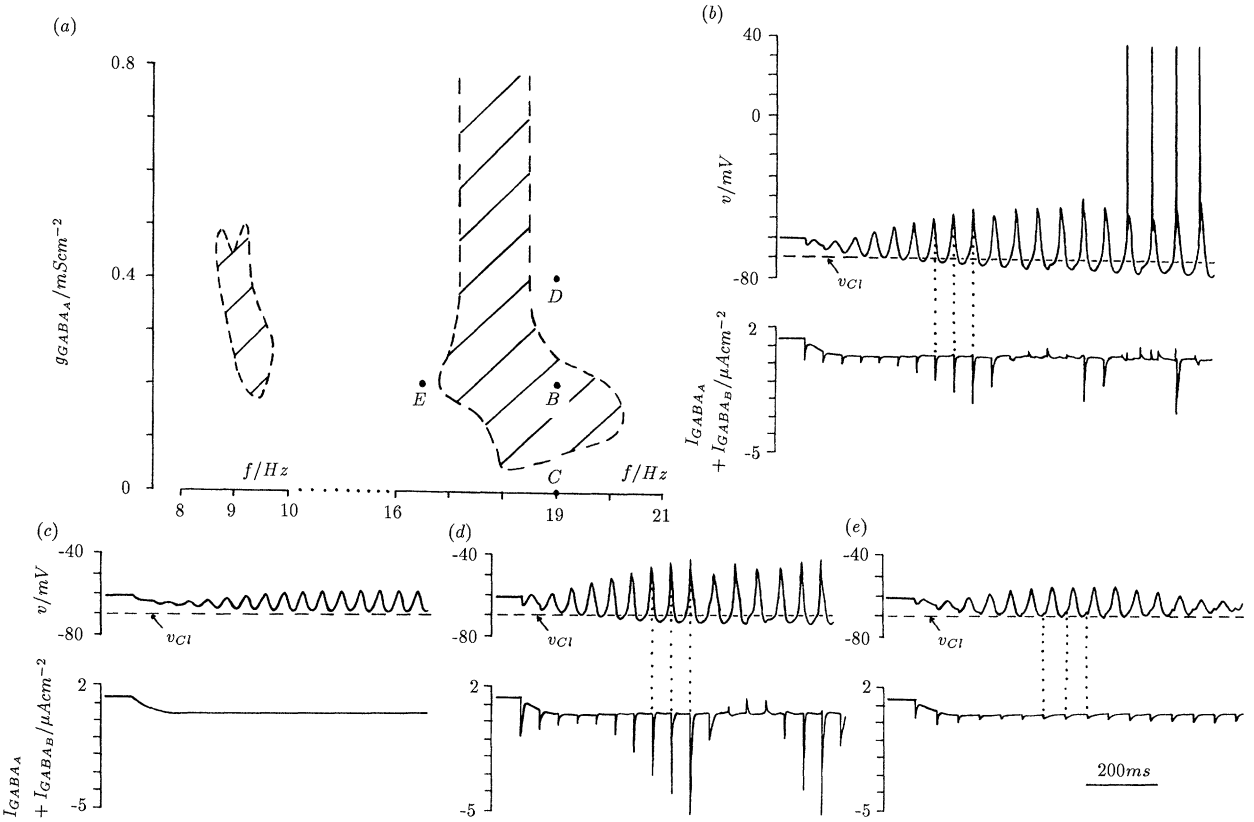

Figure 9. (*a*) (g_{GABA_A}, f) threshold tuning curves for the six-dimensional TC model (equations (14)) driven by $GABA_A$ and $GABA_B$ IPSPs as described in § 11, with $I_{Ext} = 1.4\,\mu A\,cm^{-2}$, $g_{GABA_B} = 2.2\,mS\,cm^{-2}$ and $N = 100$. The hatched regions are the values of f and g_{GABA_A} for which the cell fired action potentials, and consist of a main resonance curve at ≈ 18 Hz with a harmonic at ≈ 9 Hz. (*b*)–(*e*) Timecourses of membrane potential (upper traces) and of $I_{GABA_A} + I_{GABA_B}$ (lower trace) for points B–E respectively in (*a*). In (*b*) $g_{GABA_A} = 0.2\,mS\,cm^{-2}$ and $f = 19$ Hz. In (*c*) $g_{GABA_A} = 0\,mS\,cm^{-2}$ and $f = 19$ Hz. In (*d*) $g_{GABA_A} = 0.4\,mS\,cm^{-2}$ and $f = 19$ Hz. In (*e*) $g_{GABA_A} = 0.2\,mS\,cm^{-2}$ and $f = 16.5$ Hz. For further explanation see text.

PHILOSOPHICAL TRANSACTIONS OF THE ROYAL SOCIETY B BIOLOGICAL SCIENCES

threshold spike as in figure 9*d* (where $f = 19\,\mathrm{Hz}$ and $g_{\mathrm{GABA_A}} = 0.4\,\mathrm{mS\,cm^{-2}}$).

These results show how the apparently small $\mathrm{GABA_A}$ IPSPs (with an equilibrium potential close to rest) could have a large effect on the buildup of oscillations for points inside the tuning curves.

12. DISCUSSION

Our view is that it is likely that spindle generation by cat TC cells is the result of a cyclical movement around an inverted bifurcation diagram. There appear to be two principal ways in which this cyclical movement could take place. The first, described by our simple four-dimensional model of §§ 2 and 5 is an elaboration of the model discussed in the previous papers (Hindmarsh & Rose 1994*a*,*b*). The second, described by the four-dimensional model of § 8, is a simplification of the nine-dimensional model discussed by Destexhe *et al.* (1993). In this model periodic motion takes place around an inverted bifurcation diagram in the (v, s) plane, where s is the slow variable of the current I_{H}. As we have remarked in the Introduction, in their model the effect of adding I_{H} is both to invert a previously non-inverted bifurcation diagram and to provide a mechanism (the variation of s) to generate the cyclical movement around this diagram. Our experience is that choosing parameter values so that I_{H} performs this dual function is a delicate matter.

In the our model the bifurcation diagram, in the (v, I) plane, is already inverted by $I_{\mathrm{KCa(T)}}$ before the addition of I_{H}. The system can be driven around this bifurcation diagram using an m_{H} variable with a fixed time constant (as in the simple model of § 5) or using a two variable (s, f) description of I_{H} (equations (13) or (14)). We think that inverting the bifurcation diagram independently of I_{H} makes the model more robust. Our final model (figure 7) also appears to bear a closer resemblance to the experimental recordings than the model of Destexhe *et al.* (1993). For instance their model has large amplitude LTSs and shows marked oscillations during the inter-spindle period. Neither of these features occur in the real cell (Soltez *et al.* 1991).

The main argument against our model of spindling is that $I_{\mathrm{KCa(T)}}$ is reported to be small or negligible in thalamocortical cells (McCormick & Pape 1990*a*). Note, however, that less than thirty percent of cat thalamocortical cells generate intrinsic spindles (Soltez *et al.* 1991) and to disprove our model it would be necessary to show that $I_{\mathrm{KCa(T)}}$ was absent in a cell that was already spindling. We would expect it to be absent in a cell that was not generating spindles. Furthermore we have shown (Hindmarsh & Rose 1994*a*) that it only requires a small $I_{\mathrm{KCa(T)}}$ to invert the bifurcation diagram and so provide conditions for spindle generation. Voltage clamp experiments need to be carried out on spindling TC cells to determine whether or not this current is present.

Since the equations of our model are simpler than the nine-dimensional system of Destexhe *et al.* (1993) we have been able to predict analytically the existence of resonance (driven spindling as in §§ 6 and 7) in these cells. This prediction depended on the presence of an inverted bifurcation diagram. Whichever model is closer to reality it is significant that both models have inverted bifurcation diagrams. This makes it likely that such resonance effects could be demonstrated experimentally. For example if a cell is generating spindles then according to our model these spindles may be terminated by a small depolarizing current leaving the cell at rest. We then predict that the cell could be driven into spindling by a periodic applied current.

This prediction of resonance in response to a sinusoidal input is not just of theoretical interest. In § 11 we have shown how the form of the bifurcation diagram and the presence of resonance near the bifurcation point can be used to suggest a new role for $\mathrm{GABA_A}$ and $\mathrm{GABA_B}$ IPSPs. We have shown that summation of slow $\mathrm{GABA_B}$ IPSPs would move the membrane potential from a resting potential on the right of the bifurcation diagram to a more negative potential which is closer to the bifurcation point. At this new potential, oscillations may be built up by $\mathrm{GABA_A}$ IPSPs whose frequency and conductance values give a point inside the tuning curves of figure 9. Note, however, that if $g_{\mathrm{GABA_B}}$ is too large the membrane potential would be driven past the bifurcation point. The EP would then become unstable and spindles would be generated. This appears to happen in the presence of bicucculine (von Krosigk *et al.* 1993). Bicucculine is known to both block $\mathrm{GABA_A}$ IPSPs and enhance $\mathrm{GABA_B}$ IPSPs (Crunelli & Leresche 1991), which would produce the effect just described.

Experiments by Steriade and coworkers (Steriade & Deschenes 1984; Steriade *et al.* 1985, 1987, 1988) and by von Krosigk *et al.* (1993) strongly suggest that the nRT is the pacemaker for the thalamic spindle rhythm. Spindle generation in the nRT could be due to network interactions alone or to network interactions combined with endogenous oscillatory properties in some cells of the network (Steriade *et al.* 1987). We predict, on the basis of the similarity to the recordings of von Krosigk *et al.* (1993) that some cells could be endogenous bursters and generate reverse spindles as described in § 10.

Since we have a model of reverse spindling in an nRT neuron, and we have suggested that TC cells may resonate to inputs from the nRT, it is appropriate to summarize the main results of this paper by constructing a minimal model of driven spindling in which a reverse spindling nRT cell drives a TC cell.

In § 10 we discussed a model of reverse spindling which consisted of the simple three-dimensional model of Hindmarsh & Rose (1994*a*, Appendix 1) with v_{sep} chosen to give a Type C bifurcation diagram and small values chosen for k and k_{Ca} to slow down the change in c. The more realistic four-dimensional model of Hindmarsh & Rose (1994*a*, Appendix 3) can be modified in a similar way. Reverse spindling for this four dimensional model with $v_{\mathrm{sep}} = 0.9\,\mathrm{mV}$, $k_{\mathrm{Ca}} = 0.000088\,\mathrm{ms^{-1}}$, $k = 0.000002\,\mu\mathrm{M\,cm^{-2}\,\mu A^{-1}\,ms^{-1}}$ and $I_{\mathrm{Ext}} = 0\,\mu\mathrm{A\,cm^{-2}}$ is shown in the upper trace of figure 10*a*, with an

PHILOSOPHICAL TRANSACTIONS OF THE ROYAL SOCIETY B BIOLOGICAL SCIENCES

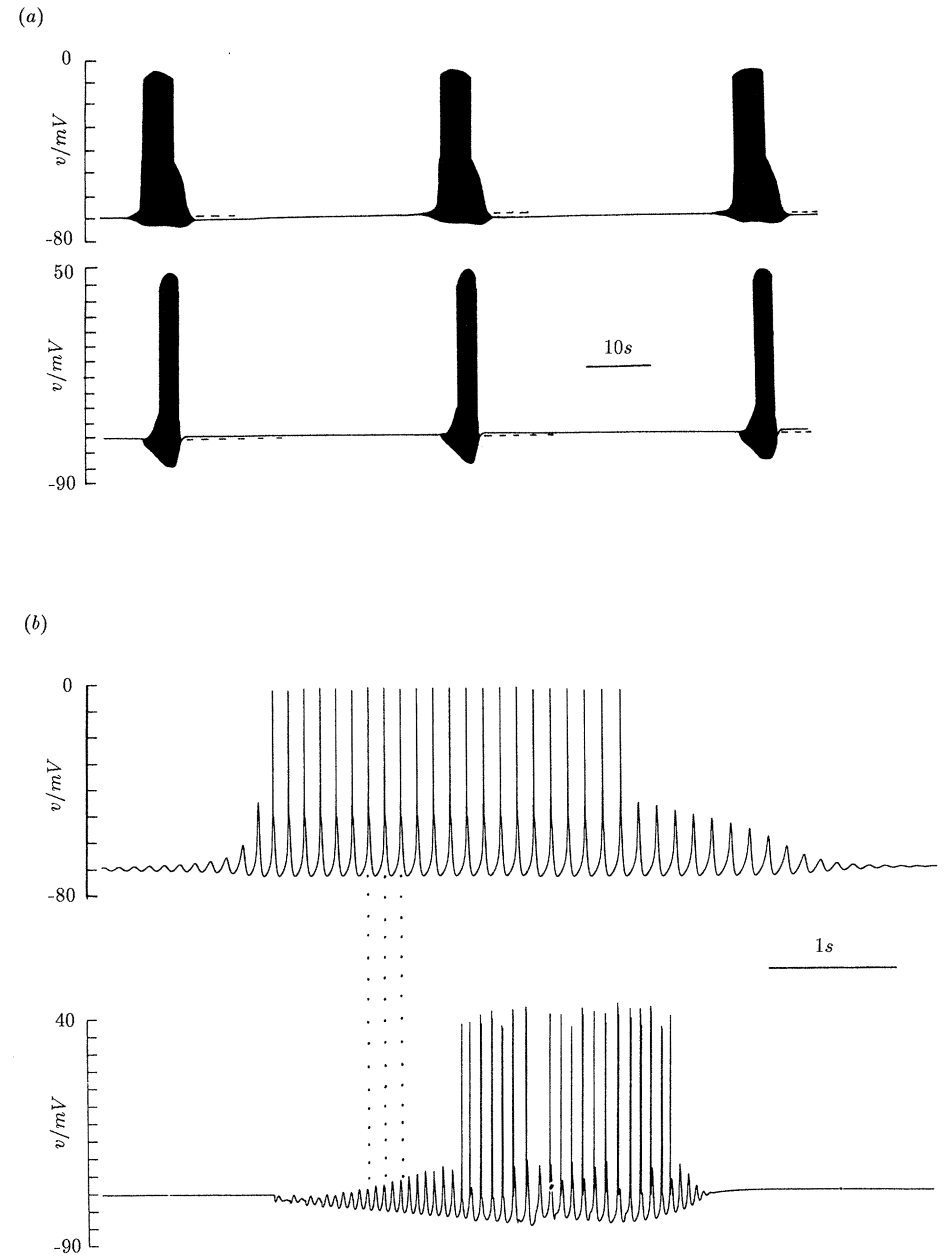

Figure 10. Minimal model of a driven spindle. (*a*) Upper trace shows membrane potential changes for the four-dimensional reverse spindle model of an nRT neuron described in the Discussion. The equations and parameter values for this model are as in Appendix 3 of Hindmarsh & Rose (1994*a*) with $v_{sep} = 0.9\,\mathrm{mV}$, $k_{Ca} = 0.000088\,\mathrm{ms}^{-1}$, $k = 0.000002\,\mu\mathrm{M\,cm}^{-2}\,\mu\mathrm{A}^{-1}\,\mathrm{ms}^{-1}$, and $\sigma_{Na} = 5\,\mathrm{mV}$. This nRT spindle drives the six-dimensional TC model shown on the lower trace. The TC model has the same equations, parameter values and tuning curves as shown in figure 9 but $g_{GABA_A} = 0.25\,\mathrm{mS\,cm}^{-2}$ and the input frequency, f, is replaced by the instantaneous intraspindle frequency, f_{Inst}, of the nRT cell. (*b*) The first nRT spindle (upper trace) and the first TC spindle (lower trace) of (*a*) shown on an expanded timescale. For further explanation see Discussion.

expanded view of the spindle in the upper trace of figure 10*b*.This spindle is similar in several respects to the spindles recorded from ferret nRT neurons by von Krosigk *et al.* (1993). In particular the frequency of spindling is similar and there is a progressive hyperpolarization during the spindle so that the cell is more hyperpolarized at the end of the spindle than at the beginning (shown by dashed lines in figure 10*a*). The depth of this post-spindle hyperpolarization is however less than in the recorded spindles.

To model a TC cell we used the six-dimensional model shown in figure 7 of this paper, using equations (14) with the parameter values given in § 9 except that the threshold for the fast action potentials was lowered by changing σ_{Na} from 10 mV to 5 mV. As we are mainly interested in the subthreshold response of the TC cell, feedback from the TC cell to the nRT cell was not included. The TC cell was coupled to the nRT cell by adding I_{GABA_A} and I_{GABA_B}, given by equations (17) and (18), to the $\dot{v}$ equation of the TC model. Parameter values for I_{GABA_A} and I_{GABA_B} were as used in the calculation of the tuning curves of figure 9*a*. In the expressions for these currents the frequency, f, was replaced by an instantaneous frequency $f_{Inst} = 1000/(t_n - t_{n-1})$, where t_n is the time of occurrence of the nth action potential in the nRT cell.

Since f_{Inst} varies between 9.85 Hz at the beginning of the reverse spindle to 8.8 Hz at the end, we chose $g_{\mathrm{GABA_A}} = 0.25\,\mathrm{mS\,cm^{-2}}$. Inspection of the tuning curves of figure 9*a* shows that with this value of $g_{\mathrm{GABA_A}}$ and with this variation of f_{Inst} there will be a horizontal movement of the parameter points from right to left across the hatched closed region that is centred around 9 Hz. The resulting driven spindle is shown in the lower traces of figure 10*a*,*b*.

This driven TC cell spindle has similarities to some of the spindles shown, for instance, in the paper by von Krosigk *et al.* (1993). However, this is the first time that it has been suggested that spindling in TC cells could be a resonant response to inputs from nRT cells. The nature of this resonant response is such that only TC cells which are themselves capable of intrinsic spindling and which have the appropriate synaptic inputs will respond. Whether the thalamo-reticular system is as richly organized as this remains to be seen, but the mechanism is consistent with the experimental observations. It is easy to see how such a subtle mechanism could have been overlooked, and these results emphasize the need for an experimental investigation of the responses of TC cells to sinusoidal inputs.

Finally we should like to restate an underlying theme of these three papers namely that having a simplified model of a physiological model allows greater understanding and aids the construction of more realistic models.

This work was supported by the Wellcome Trust. We thank Joseph Rose for assistance with computer graphics and the referees for helpful comments.

REFERENCES

Ashmore, J.F. & Attwell, D. 1985 Models of electrical tuning in hair cells. *Proc. R. Soc. Lond.* B **226**, 325–344.

Avanzini, G., de Curtis, M., Panzica, F. & Spreafico, R. 1989 Intrinsic properties of nucleus reticularis thalami neurones of the rat studied *in vitro*. *J. Physiol., Lond.* **416**, 111–122.

Buzsaki, G., Smith, A., Berger, S., Fischer, L.J. & Gage, F.H. 1990 Petit mal tremor: hypothesis of a common pacemaker. *Neuroscience* **36**, 1–14.

Crunelli, V., Haby, M., Jassik-Gerschenfeld, D., Leresche, N. & Pirchio, M. 1988 Cl^- and K^+ dependent inhibitory postsynaptic potentials evoked by interneurones of the rat lateral geniculate nucleus. *J. Physiol., Lond.* **399**, 153–176.

Crunelli, V. & Leresche, N. 1991 A role for $GABA_B$ receptors in excitation and inhibition in thalamocortical cells. *Trends Neurosci.* **14**, 16–21.

Destexhe, A. & Babloyantz, A. 1993 A model of the inward current I_h and its possible role in thalamocortical oscillations. *Neuro. Report* **4**, 223–226.

Destexhe, A., Babloyantz, A. & Sejnowski, T.J. 1993 Ionic mechanisms for intrinsic slow oscillations in thalamic relay neurons. *Biophys. J.* (In the press.)

Gutnick, M.J. & Yarom, Y. 1989 Low threshold calcium spikes, intrinsic neuronal oscillation and rhythm generation in the C.N.S. *J. Neurosci. Meth.* **28**, 93–99.

Hindmarsh, J.L. & Rose, R.M. 1994*a* A model for rebound bursting in a mammalian neuron. *Phil. Trans. R. Soc. Lond.* B **346**, 129–150. (This volume.)

Hindmarsh, J.L. & Rose, R.M. 1994*b* Resonance in a model of a mammalian neuron. *Phil. Trans. R. Soc. Lond.* B **346**, 151–163. (Preceding paper.)

Hirsch, J.C. & Burnod, Y. 1987 Synaptically evoked late hyperpolarization in the rat dorsolateral geniculate neurons *in vitro*. *Neuroscience* **23**, 457–468.

Huguenard, J.R. & Prince, D.A. 1991 A slow inactivation of a TEA-sensitive K current in acutely isolated rat thalamic relay neurons. *J. Neurophysiol.* **66**, 1316–1328.

Leresche, N., Lightowler, S., Soltez, I., Jassik-Gersherfeld, D. & Crunelli, V. 1991 Low frequency oscillatory activities intrinsic to rat and cat thalamocortical cells. *J. Physiol., Lond.* **441**, 155–174.

McCormick, D.A. & Feester, H.R. 1990 Functional implications of burst firing and single spike activity in lateral geniculate relay neurons. *Neuroscience* **39**, 103–113.

McCormick, D.A., Huguenard, J. & Strowbridge 1992 Determination of state-dependent processing in thalamus by single neuron properties and neuromodulators. In *Single neuron computation* (ed. T. McKenna, J. Davis & S. F. Zornetzer), pp. 259–290. Academic Press.

McCormick, D.A. & Pape, H.C. 1990*a* Properties of a hyperpolarization activated cation current and its role in rhythmic oscillation in thalamic relay neurons. *J. Physiol., Lond.* **431**, 291–318.

McCormick, D.A. & Pape, H.C. 1990*b* Noradrenergic and serotonergic modulation of a hyperpolarization activated cation current I_h in thalamic relay neurons. *J. Physiol., Lond.* **431**, 319–342.

Pollard, C.E. & Crunelli, V. 1988 Intrinsic membrane currents in projection cells of the cat and rat lateral geniculate nucleus. *Neurosci. Lett.* **32**, S39.

Soltez, I. & Crunelli, V. 1992 A role for low frequency, rhythmic synaptic potentials in the synchronization of cat thalamocortical cells. *J. Physiol., Lond.* **457**, 257–276.

Soltez, I., Lighthowler, S., Leresche, N. & Crunelli, V. 1989 On the properties and origin of $GABA_A$ inhibitory postsynaptic potentials recorded in morphologically identified projection cells of the cat dorsal lateral geniculate nucleus. *Neuroscience* **33**, 23–33.

Soltez, I., Lightowler, S., Leresche, N., Jassik-Gerschenfeld, D., Pollard, C.E. & Crunelli, V. 1991 Two inward currents and the transformation of low frequency oscillations of rat and cat thalamocortical cells. *J. Physiol., Lond.* **441**, 175–197.

Steriade, M. & Deschênes, M. 1984 The thalamus as a neuronal oscillator. *Brain Res. Rev.* **8**, 1–63.

Steriade, M., Deschênes, M., Domich, L. & Mulle, C. 1985 Abolution of spindle oscillations in thalamic neurons disconnected from the reticularis thalami. *J. Neurophysiol.* **54**, 1473–1497.

Steriade, M., Domich, L., Oakson, G. & Deschênes 1987 The deafferented reticular thalamic nucleus generates spindle rhythmicity. *J. Neurophysiol.* **57**, 260–273.

Steriade, M. & Llinás, R. 1988 The functional states of the thalamus and the associated neuronal interplay. *Physiological Reviews* **68**, 649–742.

von Krosigk, M., Bal, T. & McCormick, D.A. 1993 Cellular mechanisms of a synchronized oscillation in the thalamus. *Science, Wash.* **261**, 361–364.

Wang, X-J. 1994 Multiple dynamical modes of thalamic relay neurons: rhythmic bursting and intermittent phase-locking. *Neuroscience* **59**, 21–31.

Wilcox, K.S., Gutnick, M.J. & Christoph, G.R. 1988 Electrophysiological properties of neurons in the lateral habenula nucleus: an *in vitro* study. *J. Neurophysiol.* **59**, 212–225.

Yarom, Y. 1991 Rhythmogenesis in a hybrid system-interconnecting an olivary neuron to an analog network of coupled oscillators. *Neuroscience* **44**, 263–275.

Received 3 February 1994; accepted 3 May 1994

PHILOSOPHICAL TRANSACTIONS OF THE ROYAL SOCIETY B BIOLOGICAL SCIENCES